Published in final edited form as:
Nat Genet. 2019 July 04; 51(8): 1283–1294. doi:10.1038/s41588-019-0471-2.

DNA crosslink repair safeguards genomic stability during pre-meiotic germ cell development

Ross J Hill[1] **Gerry P Crossan**[1,*]

[1]MRC Laboratory of Molecular Biology, Cambridge, UK

Abstract

Germline *de novo* mutations are the basis of evolutionary diversity but also of genetic disease. However, the molecular origin, mechanisms and timing of germline mutagenesis are not fully understood. Here, we define a fundamental role for DNA interstrand crosslink repair in the germline. This repair process is essential for primordial germ cell (PGC) maturation during embryonic development. Inactivation of crosslink repair leads to genetic instability that is restricted to PGCs within the genital ridge during a narrow temporal window. Having successfully activated the PGC transcriptional program, a potent quality control mechanism detects and drives damaged PGCs into apoptosis. These findings therefore define a source of DNA damage and the nature of the subsequent DNA repair response in germ cells, which ensures faithful transmission of the genome between generations.

Introduction

Germ cells are tasked with faithfully transmitting genetic information from one generation to the next[1]. Genomic alterations that arise in the germline, known as *de novo* mutations, can take a variety of forms: from single-nucleotide changes, to insertions and deletions, or large structural rearrangements. The precise mutagenic outcome is determined by the nature of the DNA damage and how it is processed by the repair machinery. Despite considerable knowledge about how the plethora of DNA repair pathways process specific lesions, little is known about the sources of damage or the activity of repair pathways in the mammalian germline.

The earliest mammalian germ cells, known as primordial germ cells (PGCs), emerge during early embryonic development. These cells undergo extensive epigenetic reprogramming before ultimately entering into meiosis[2]. In females, PGCs enter into meiosis during

*correspondence: gcrossan@mrc-lmb.cam.ac.uk.

Data availability statement
The data that support the findings of this study are available from the corresponding author upon request.

Author Contributions
G.P.C. and R.J.H. conceived the study, designed experiments and wrote the paper. R.J.H. performed all experiments.

Competing interests
The authors declare no competing interests.

Europe PMC Funders Author Manuscripts

embryonic development but in males the PGCs differentiate into a self-renewing stem cell population that enters meiosis postnatally. Mutations that occur in differentiated germ cells either during spermatogenesis or meiosis are likely confined to an individual offspring. However, mutations that occur in the early PGC population have the potential to be passed to multiple progeny. Therefore, the stage of germ cell development during which *de novo* mutations arise can play an important role in determining the overall fidelity of genome transmission between generations.

In order to understand the origin of *de novo* mutations it is also important to understand the molecular mechanisms that give rise to changes in the sequence and structure of the genome. The DNA repair machinery must be tightly regulated because whilst it has the capacity to detect and accurately repair damage to the genome, the DNA repair machinery also has the ability to introduce mutations and structural abnormalities in the genome. One very significant threat to germline genomic stability is meiotic recombination. Failure of meiotic recombination often results in catastrophic karyotypic abnormalities that are incompatible with life. Recently, however, the role of DNA repair proteins in PGCs has become of significant interest as one repair pathway, known as base excision DNA repair, was found to play a key role in epigenetic reprogramming events that occur in PGCs[3–5].

Data from the sequencing of cancer genomes have revealed a surprisingly large spectrum of tissue-specific mutational patterns[6–8]. This is likely to represent the interplay between tissue-specific exposure to mutagens and tissue-specific differences in DNA repair capacity. Despite the importance of understanding the origin of germline mutations, little is understood about the sources of DNA damage or repair transactions that occur in the developing germline.

Therefore, significant questions remain about the temporality, source of damage and nature of repair transactions that are active in the germline. These factors ultimately act to shape the evolution of genomes. Here we find that disabling DNA crosslink repair, which is defective in the human disease Fanconi anemia (FA), is critical for the production of viable gametes. We show that crosslink repair is required for embryonic germ cell development prior to entry into meiosis. Loss of crosslink repair leads to genomic instability within the developing PGCs but repair-deficient PGCs are efficiently cleared through apoptosis potentially limiting their ability to pass mutations on to the next generation.

Results

ERCC1 is required for normal fertility

In order to study the role of DNA repair in preventing loss of genetic stability in the germline, we focused on the structure-specific endonuclease XPF-ERCC1. This heterodimeric enzyme cleaves DNA at sites of damage to ensure its accurate repair. XPF-ERCC1 is evolutionary conserved, and plays an important role in sexual reproduction. It is known to regulate the frequency of meiotic crossover in fission yeast, flies and nematode worms, presumably due to its role in the resolution of recombination intermediates[3,9–13]. To explore the role of XPF-ERCC1 in mammalian germ cells we generated *Ercc1*-deficient mice (*Ercc1*$^{tm1a(KOMP)Wtsi}$) on a C57BL/6J genetic background. We derived *Ercc1*$^{-/-}$

embryonic fibroblasts and found that ERCC1 protein was undetectable and that these cells were hypersensitive to DNA damage (Supplementary Fig. 1a-e). We intercrossed *Ercc1*$^{+/-}$ mice and genotyped all living progeny at 14-days old (P14). As previously reported, *Ercc1*$^{-/-}$ mice were severely underrepresented (1.9% compared to the expected 25% at P14) and all had died by 21-days old[14,15] (Supplementary Fig. 1f-g).

At P14, we found that there was an obvious reduction in the number of oocytes and spermatogenic cells in the gonads of *Ercc1*$^{-/-}$ pups (Fig. 1a-f). *Ercc1*$^{-/-}$ females had a 9.5-fold reduction in the number of oocytes compared to congenic wildtype controls (Fig. 1b). Despite this large reduction in the number of oocytes there was only a modest 1.6-fold reduction in the mass of the ovaries (Supplementary Fig. 1h). Strikingly, most seminiferous tubules in *Ercc1*$^{-/-}$ males lacked germ cells (Fig. 1c). In agreement with this, *Ercc1*$^{-/-}$ males had a significant reduction in the number of cells expressing PLZF, a marker of early spermatogenic cells (6.1-fold, Fig. 1a and d)[16]. We noticed that the reduction in the number of PLZF^{+} cells was not uniform among all seminiferous tubules. In the absence of ERCC1, the vast majority of tubules had no PLZF^{+} cells (Fig. 1e), but the few remaining seminiferous tubules contained normal numbers of PLZF^{+} cells compared to wildtype controls (Fig. 1f). This led us to question if the pool of cells that embryonically seeded the seminiferous tubules could have been reduced. We employed mouse vasa homologue (MVH), a marker of germ cells, to measure the numbers of germ cells in the embryonic gonads at day 18.5 of development (E18.5). Both female and male *Ercc1*$^{-/-}$ embryos had significant reductions in the numbers of MVH^{+} germ cells compared to wildtype controls (11.1-fold and 9.3-fold, respectively Fig. 1g,h and Supplementary Fig. 2a,b). This was intriguing, as whilst female germ cells have already entered meiosis at E18.5 male germ cells have not, suggesting a common pre-meiotic origin to the germ cell defect in both males and females. We next assessed the E18.5 gonads for evidence of apoptosis. We could not detect a significant increase in the frequency of apoptotic (cleaved-Caspase 3^{+}) cells in either *Ercc1*$^{-/-}$ male or female gonads (Supplementary Fig. 2c,d). When we looked specifically at germ cells (MVH^{+}) we could find no cleaved-Caspase 3^{+} cells (from a total of 149 MVH^{+} germ cells). Taken together these data suggest that the reduction in germ cells observed in both male and female *Ercc1*$^{-/-}$ mice precedes meiosis.

A critical role for DNA repair in primordial germ cell development

We therefore set out to test if ERCC1 was required in the earlier PGC pool. We intercrossed *Ercc1*$^{+/-}$ mice with a PGC-reporter mouse in which the expression of GFP is driven by a fragment of the *Oct4* (*Pou5f1*) promoter (known as *GOF18-GFP*) on a C57BL/6J background[17,18]. At E13.5 the gonads of *Ercc1*$^{-/-}$ embryos had a dramatic reduction in the number of PGCs when compared to wildtype littermates (Fig. 2a). We quantified this defect by flow cytometry and found that in the absence of ERCC1 there was there was a 10.0-fold reduction in the number of PGCs (SSEA1^{+}GOF18-GFP^{+}) (Fig. 2b,c). At E13.5, female PGCs are entering into meiosis, a process that does not occur in males until after birth. We therefore hypothesized that if the loss of PGCs were due to entry into meiosis, then we would find a female-specific reduction in PGCs. However, we found that both *Ercc1*$^{-/-}$ males and females had similar reductions in the number of PGCs at E13.5 (Fig. 2d). Female *Ercc1*$^{-/-}$ embryos had an 8.7-fold reduction in the number of PGCs when compared to

wildtype female embryos at E13.5. Comparably, ERCC1-deficient males had a 9.2-fold reduction in the number of PGCs compared to wildtype males. This pointed to a common defect in both males and females leading to the reduction in PGCs.

We next examined the frequency of PGCs at E12.5 by which point neither males nor females have yet entered meiosis. We found that *Ercc1*$^{-/-}$ embryos had a 10.6-fold reduction in the frequency of PGCs, respectively (Fig. 2c). Both males and females exhibited comparable reductions in the number PGCs (Fig 2d). To ensure that this defect was not an artefact of the *GOF18-GFP* reporter we crossed *Ercc1*$^{+/-}$ mice with an alternative PGC reporter, *Stella-GFP*[19], and found that at E12.5 *Ercc1*$^{-/-}$ embryos had similar reductions in the number of PGCs with both reporters (Supplementary Fig. 3a).

To determine when during PGC development the defect began we analyzed embryos between E9.5 and E13.5. We found that between E11.5-13.5 *Ercc1*-deficient embryos had significantly reduced numbers of PGCs compared to wildtype littermates (Fig. 2e, Supplementary Fig. 3b). It is noteworthy that the 10.6-fold reduction first observed in PGCs at E12.5 is similar in magnitude to the reduction in MVH^{+} germ cells at E18.5. This strongly suggests that the major reduction of germ cells in *Ercc1*$^{-/-}$ mice occurred before E12.5.

Finally, we crossed a conditional allele of *Ercc1* with a Cre recombinase expressed in early PGCs (*Blimp1-Cre*[20]). We found that loss of ERCC1 in PGCs resulted in an almost complete loss of gamete production in both males and females (Fig. 2f). The histological appearance was consistent with the defects observed in 14-day old constitutive *Ercc1*$^{-/-}$ pups. 8- to 12-week old *Ercc1*$^{-/f}$*Blimp1-Cre*$^{+}$ males showed a significant reduction of PLZF^{+} cells per tubule (Supplementary Fig. 3c and d) similar in magnitude to the reduction observed in *Ercc1*$^{-/-}$ constitutive knockout mice at P14 (7.3-fold and 6.1-fold, respectively). When either male or female *Ercc1*$^{-/f}$*Blimp1-Cre*$^{+}$ mice were crossed with wildtype mates they failed to give rise to offspring despite evidence of copulation (Fig. 2g, Supplementary Fig. 3e and f). These data show that there is a critical requirement for ERCC1 in preserving normal numbers of PGCs prior to entry into meiosis.

ERCC1 acts with the Fanconi pathway to preserve PGC development

XPF-ERCC1 plays a critical role in multiple DNA repair transactions. It is essential for both global genome and transcription-coupled nucleotide excision repair (GG- and TC-NER). XPF-ERCC1 also plays an important role in a subset of homologous recombination transactions[21]. In addition, it is also a critical factor in the Fanconi-mediated repair of DNA interstrand crosslinks (ICLs)[22,23]. It is therefore possible that the PGC defect observed in *Ercc1*$^{-/-}$ mice is due to loss of one of these individual repair functions or the simultaneous inactivation of multiple routes of DNA repair.

In order to discriminate between these possibilities, we decided to focus our attention on pathway-specific factors. FANCA is a component of the Fanconi-mediated DNA interstrand crosslink repair pathway while XPA interacts with XPF-ERCC1 segregating its function in NER. We first assessed the expression of *Ercc1*, *Fanca* and *Xpa* in E12.5 PGCs by qRT-PCR (Fig. 3a). We found that the levels of *Ercc1*, *Fanca* and *Xpa* expression were higher in PGCs compared to surrounding somatic cells (SSEA1^{-}GOF18-GFP^{-}). The expression of both

Ercc1 and *Fanca* increased similarly during PGC development (E8.5-E12.5), peaking at E10.5, whilst the expression of *Xpa* was relatively constant (Fig. 3b).

We compared the phenotypes of mice deficient in ERCC1 with those deficient in either FANCA or XPA. The ovaries and testes of *Xpa*$^{-/-}$ mice were examined at P14 and found to be indistinguishable from wildtype controls (Fig. 3c). In contrast, *Fanca*$^{-/-}$ males and females showed little evidence of spermato- or oogenesis, reminiscent of *Ercc1*$^{-/-}$ mice (Fig. 3c). We went on to examine the phenotypes of sexually mature mice (8-12 weeks old), but employed conditional *Ercc1*$^{-/f}$*Blimp1-Cre*$^{+}$ mice as the constitutive knockout mice die before reaching sexual maturity. To fully exclude a role of NER we extended our analysis to *Csb*$^{-/-}$ mice (deficient in TC-NER). We found both XPA- and CSB-deficient adults were fertile (Supplementary Fig. 4a and b). In contrast, FANCA-deficient mice were infertile with ovaries and testes that were largely devoid of germ cells (Supplementary Fig. 4a-e). These histological features and fertility defects closely resemble what was observed in *Ercc1*$^{-/f}$*Blimp1-Cre*$^{+}$ mice (Supplementary Fig. 4c-e).

These data suggested that it is XPF-ERCC1's role in crosslink repair that is critical to ensure normal germ cell development. Fertility defects in mice and humans deficient in the Fanconi-mediated crosslink repair pathway have been documented [24–27]. Previous studies have suggested important roles for several Fanconi proteins in both meiosis and PGC proliferation, but the basis of this infertility remains poorly understood[24,25,28–32]. Although the data presented here clearly show that in the absence of ERCC1 a PGC defect precedes the onset of meiosis, we did analyze meiosis in mice deficient in either ERCC1 or FANCA (Supplementary Note and Supplementary Figs. 5 and 6). These data reveal that whilst the loss of crosslink repair initially delays progression through meiosis it is not essential for the production of functional gametes[33–37].

In the absence of ERCC1, germ cell defects are observed at E11.5, prior to meiosis. To test if FANCA, like ERCC1, is required for pre-meiotic PGC development we generated mouse embryonic stem cells (mESCs) that lacked ERCC1 or FANCA and carried the *GOF18-GFP* reporter (Supplementary Fig. 7a and b). In the absence of ERCC1 or FANCA mESCs were defective at differentiating into primordial germ cell-like cells (PGCLCs) *in vitro* (Supplementary Fig. 7c and d). It is worth noting that day 4 PGCLCs are likely to correspond to early stages of PGC development[38–41]. It is therefore interesting that we find a requirement for crosslink repair in PGCLC formation given that we observe only a modest reduction in the number of PGCs at early time points. This highlights the importance of *in vivo* models to study the role of DNA repair in PGC development.

We therefore set out to test the requirement for FANCA *in vivo* by crossing *Fanca*$^{+/-}$ mice with the GOF18-GFP reporter. We examined the gonads of E12.5 *Fanca*$^{-/-}$ embryos and observed a significant 7.9-fold reduction in the numbers of PGCs when compared to wildtype littermates (Fig. 3d and e). The number of PGCs observed in *Fanca*$^{-/-}$ embryos was also comparable to the number observed in *Ercc1*$^{-/-}$ embryos (Fig. 3e) and no difference could be found in the magnitude of the PGC defect between males and females (Supplementary Fig. 8a and b). Similar to ERCC1-deficiency we observed that the primordial germ cell defect emerged between E10.5 and E12.5 (Fig. 3f).

To test if ERCC1 and FANCA act together to preserve the number of PGCs we generated *Ercc1*$^{-/-}$*Fanca*$^{-/-}$ embryos. We found that loss of FANCA did not further exacerbate the PGC defect observed in *Ercc1*$^{-/-}$ embryos at day E12.5, revealing that ERCC1 and FANCA work in the same pathway to preserve PGC development (Fig. 3g).

This suggests that there may be a particular requirement for DNA ICL repair during PGC development. To test if the requirement was generalizable to other factors involved in ICL repair we extended our analysis to SLX4 and FAN1. SLX4 directly interacts with XPF-ERCC1 to promote incisions at sites of crosslinked DNA, whilst FAN1 acts in a parallel pathway to XPF-ERCC1[23,42–44]. We found that whilst SLX4-deficient mice have a profound fertility defect akin to *Fanca*$^{-/-}$ and *Ercc1*$^{-/f}$*Blimp1-Cre*$^{+}$, *Fan1*$^{-/-}$ mice were fertile (Supplementary Fig. 9a and b). At E12.5 *Fan1*$^{-/-}$ embryos had an intact germ cell compartment (Supplementary Fig. 9c). This shows that whilst Fanconi-mediated DNA repair is required for germ cell development this requirement is not generalizable to all routes of ICL repair.

Surviving crosslink-repair-deficient PGCs undergo specification and epigenetic reprogramming

In order to determine the fate of FA crosslink repair-deficient PGCs we examined their phenotype in more detail. We measured the expression of PGC markers in early (E10.5) and late (E12.5) genital ridge PGCs. We found that in the absence of crosslink repair PGCs had indistinguishable expression of early (*Ap2γ*, *Prdm14*, *Blimp-1* and *Stella*) and late (*Mvh* and *Dazl*) PGC markers when compared to wildtype PGCs (Fig. 4a, Supplementary Fig. 9d)[45,46]. This suggests that the PGC specification program is intact in the remaining crosslink-repair-deficient PGCs.

We set out to assess if crosslink repair deficiency perturbed PGC migration[47–49]. Firstly, we found that when quantified microscopically the PGC defect in ERCC1-deficient embryos was consistent with our findings by flow cytometry (Supplementary Figs. 10, 11 and Fig. 2e). Secondly, at E9.5 and E10.5 *Ercc1*$^{-/-}$ PGCs (GOF18-GFP^{+}) were similarly distributed compared to wildtype controls, with no evidence of an increase in the frequency of ectopically localized PGCs (Supplementary Fig. 10a-g). Furthermore, at E11.5 the few remaining *Ercc1*$^{-/-}$ PGCs were exclusively located within the genital ridge (Supplementary Fig. 11a-c).

In the genital ridge PGCs undergo a process of epigenetic reprogramming, we therefore asked if key events in this process occurred normally in crosslink-repair-deficient PGCs. Early epigenetic reprogramming in PGCs results in altered histone modifications. We assessed PGCs for trimethylation of histone H3 at lysine 27 (H3K27me3 – high levels of which are acquired in PGCs) and dimethylation of histone H3 at lysine 9 (H3K9me2 – which is erased in PGCs)[5,50,51]. We found no difference in either H3K27me3 or H3K9me2 at a global level in crosslink-repair-deficient PGCs when compared to wildtype controls (Fig. 4b,c). We went on to determine if DNA demethylation and imprint erasure occurred in the absence of DNA crosslink repair. We assessed the level of DNA methylation at a series of genomic loci. PGCs (SSEA1^{+}GOF18-GFP^{+}) and surrounding somatic cells (SSEA1^{-} GOF18-GFP^{-}) were isolated by flow cytometry from E12.5 embryos and used for sodium

bisulphite sequencing. We assessed the methylation of *Tex19.1* and *Mili* (germline factors dependent on promoter demethylation), *H19* (an imprinted locus) and *Line1* (transposable element) [46,52,53]. In all cases we found that at E12.5 *Ercc1*$^{-/-}$ and *Fanca*$^{-/-}$ PGCs had erased methylation to the same extent as wildtype PGCs (Fig. 4d,e, Supplementary Figs. 12 and 13). Together these data suggest that in the absence of crosslink repair key events in PGC specification and epigenetic reprogramming occur normally in the remaining PGCs.

Repair-deficient PGCs accumulate unrepaired DNA double strand breaks

We hypothesized that in the absence of crosslink repair PGCs may accumulate unrepaired DNA damage. As the reduction in the number of PGCs occurred between E10.5-E12.5 we chose to assess E11.5 embryos for evidence of DNA damage. We measured 53BP1 (a surrogate marker of DNA double strand breaks, DSBs) and γ-H2A.X focus formation (an alternative, albeit less specific, marker of DSBs). In the absence of either ERCC1 or FANCA a greater proportion of PGCs showed elevated levels of DSB markers (Fig. 5a and b). To directly measure DSBs in PGCs, we employed single-cell gel electrophoresis on FACS-purified PGCs from E11.5 *Ercc1*$^{-/-}$, *Fanca*$^{-/-}$ and wildtype embryos. In the absence of either FANCA or ERCC1 there was a significant induction in comet tail moment (Fig. 5c). To assess if these PGCs were undergoing replication, we pulsed pregnant females with EdU and found that both *Ercc1*$^{-/-}$ and *Fanca*$^{-/-}$ PGCs incorporated EdU to a similar extend as wildtype PGCs (Supplementary Fig. 14a).

Finally, we charted the accumulation of DSB formation during PGC development in *Fanca*$^{-/-}$ embryos. We found that E11.5 embryos had the highest frequency of γ-H2A.X^{+} PGCs (Fig. 5d). Interestingly, the maximum induction of DNA damage coincides with the period during which the reduction in PGC number occurred (Fig. 5d,e). DNA damage did not correlate with the global levels of H3K27me3 or H3K9me2 levels in PGCs (Supplementary Fig. 14b-e). These data show that crosslink-repair-deficient PGCs are lost within a narrow temporal window during which they accumulate unrepaired DNA DSBs.

Aldehyde detoxification preserves germ cell genome stability

Although we have shown that the Fanconi pathway and XPF-ERCC1 act together to prevent the loss of genome stability in PGCs, it is unclear what causes the initial DNA damage. It has recently been reported that metabolically produced aldehydes can cause mutagenesis and cell death within Fanconi-deficient hematopoietic stem cells[54–58]. Reactive aldehydes (such as formaldehyde and acetaldehyde) can cause DNA interstrand crosslinks but can also cause a plethora of other DNA lesions, including base adducts, intrastrand- and protein-DNA crosslinks.

We therefore set out to test if sufficient acetaldehyde or formaldehyde is generated during fetal development to perturb *Fanca*$^{-/-}$ PGC development. In order to do this we employed mice deficient in either ALDH2 (required for acetaldehyde catabolism) or ADH5 (required for formaldehyde catabolism.) This allowed us to generate embryos deficient in both Fanconi-mediated crosslink repair and aldehyde catabolism, *Aldh2*$^{-/-}$*Fanca*$^{-/-}$ or *Adh5*$^{-/-}$ *Fanca*$^{-/-}$ that carried the *GOF18-GFP* reporter (Fig. 6a). The gonads of E12.5 *Aldh2*$^{-/-}$ *Fanca*$^{-/-}$ and *Adh5*$^{-/-}$*Fanca*$^{-/-}$ embryos had fewer PGCs compared to the *Fanca*$^{-/-}$ single

mutant (Fig. 6b-d).This further reduction in the number of PGCs is accompanied by a concomitant increase in the proportion of PGCs carrying markers of damaged DNA (Fig. 6e).

It is worth noting that ALDH2 and ADH5 cannot compensate for each other in protecting developing germ cells from reactive aldehydes. These data show that sufficient aldehydes (substrates of ALDH2 or ADH5) are generated within the developing fetus to compromise the PGC population at least when the FA pathway is defective, defining endogenous reactive aldehydes as mutagens that can corrupt the genome of the developing germ line. As 540 million people carry inactivating mutations of *Aldh2*, exposure of developing germ cells to elevated levels of acetaldehyde may be common in the human population[59].

Damaged PGCs are efficiently cleared through apoptosis

We next questioned if the accumulation of damaged DNA is specific to PGCs or is widespread in FA crosslink-repair-deficient embryos. We assessed γ-H2A.X and 53BP1 focus formation in both the PGCs (GOF18-GFP^{+}) and also surrounding somatic cells (GOF18-GFP^{-}) of the developing gonad at E11.5. As already shown, both *Ercc1*$^{-/-}$ and *Fanca*$^{-/-}$ embryos had significant increases in the frequency of γ-H2A.X- or 53BP1-positive PGCs (Fig. 5a and b). Surprisingly, in somatic cells there was no difference in the accumulation of these DNA DSB markers between crosslink repair-deficient and wildtype littermates (Fig. 7a and b).

The failure to accurately repair DNA DSBs leads to the loss of genome stability and mutation. We therefore wanted to ask how PGCs are prevented from passing on mutagenized genetic material to the next generation. We found that in the absence of either FANCA or ERCC1, PGCs accumulated a phosphorylated form of p53 (pSer15-p53) (Fig. 7c). Given the dramatic reduction in PGC number we hypothesized that they may be lost through p53-dependent apoptosis. *Ercc1*$^{-/-}$ and *Fanca*$^{-/-}$ embryos had increased frequency of apoptotic PGCs compared to littermates (cleaved-Caspase 3^{+}, 7.7-fold and 7.4-fold, respectively) (Fig. 7d). Of the PGCs that carried evidence of unrepaired DNA DSBs (persistent γ-H2A.X) we found that a large proportion of these cells were also positive for pSer15-p53 (Supplementary Fig. 15). Together these data show that crosslink repair-deficient PGCs accumulate DNA damage, pSer15-p53, and enter into apoptosis.

Discussion

Germ cells are single-handedly tasked with passing genetic information from one generation to the next, it is therefore of paramount importance that these cells maintain the integrity of their genomes. We use constitutive knockout mice to show that in the absence of ERCC1 or FANCA germ cell defects precede meiosis. The loss of PGCs occurs between E10.5 and E12.5, which is before either male or female germ cells enter into meiosis. The results presented here reveal that in the absence of FA crosslink repair PGCs accumulate DSBs, undergo apoptosis and are lost prior to entry into meiosis. This sheds new light on the nature of DNA damage, repair processes and quality control mechanisms that prevent *de novo* germline mutagenesis.

Whilst XPF-ERCC1 is required for many different DNA repair transactions, FANCA is restricted to a role in the Fanconi ICL repair pathway. We find that the magnitude and temporality of PGC loss is similar between *Ercc1*$^{-/-}$ and *Fanca*$^{/-}$ embryos. Most strikingly, we find that *Ercc1*$^{-/-}$*Fanca*$^{-/-}$ embryos have a PGC defect that is indistinguishable from either of the single mutants. These data reveal that XPF-ERCC1 acts together with the Fanconi DNA repair pathway in order to ensure normal PGC development. In contrast, whilst FAN1 is required to maintain cellular resistance to crosslinking agents, we find that it is dispensable for PGC development. Hence, PGCs have a specific requirement for Fanconi-mediated DNA interstrand crosslink repair to ensure normal development.

Crosslink-repair-deficient PGCs accumulate unresolved DNA breaks that can lead to cell death or, if illegitimately repaired, insertions, deletions or structural changes. Therefore, the role of DNA crosslink repair in suppressing germline DNA DSBs is critical to maintain germline genome stability. It is worth noting that whilst crosslink-repair-deficient PGCs accumulate unresolved DSBs, the surrounding somatic cells do not exhibit elevated levels of DNA damage. It has been suggested that PGCs have different responses to DNA damage compared to somatic cells[60], however, the fact that PGCs specifically accumulate damaged DNA strongly suggests the PGCs face unique threats to their genetic integrity, necessitating crosslink repair. The observation that crosslink-repair-deficient PGCs accumulate stabilized p53 and enter into apoptosis during the period in which they exhibit elevated levels of DNA damage may provide a simple mechanism to prevent the transmission of corrupted genetic information to the next generation (Supplementary Fig. 16).

Crosslink repair is crucial during a narrow temporal window (E10.15-E12.5) coinciding with PGC epigenetic reprogramming and expansion. It is plausible that the epigenetic reprogramming could in-itself pose a threat to genome integrity when crosslink repair is inactivated. It is worth noting that in the absence of FA crosslink repair there is a significant defect in the ability to generate induced pluripotent stem cells (iPSCs)[61,62]. Although by no means the same process, iPSC reprogramming does share some similarities with PGC development (activation of pluripotency markers, DNA demethylation and alterations to histone modifications)[63]. DNA demethylation, histone demethylation or retrotransposon reactivation may pose threats to genetic integrity during PGC reprogramming necessitating the FA pathway[3,64]. However, we find that in the absence of crosslink repair, the remaining PGCs have undergone the major landmarks of epigenetic reprogramming. Alternatively, PGC epigenetic reprogramming may induce a unique genomic state which when compounded by crosslink repair deficiency results in cellular toxicity. Going forward, it will be critical to uncover if there are other sources of DNA damage that pose unique threats to the genetic integrity of PGCs.

There are human patients with mutations that lead to defective FA-mediated DNA crosslink repair. In agreement with our mouse models, both male and female FA patients (including those with mutations in FANCA and FANCQ/XPF) have fertility defects[15,22,26,27,65–68]. Despite limited studies of fertility in human patients both males and females exhibit hypogonadism with hormonal dysregulation. Females have been shown to have primary ovarian insufficiency with premature menopause. The male patients reveal Sertoli cell-only tubules, the same pathological feature that we find in our mouse models. The phenotypes

reported in FA patients are consistent with germ cell loss due to failure of PGC development. This study provides a plausible explanation for the infertility observed in human patients with FA. More generally, this work suggests that the process of embryonic germ cell development may pose unique challenges to the DNA damage repair machinery.

Methods

Mice

All animal experiments undertaken in this study were with approval of the MRC Laboratory of Molecular Biology animal welfare and ethical review body and the UK Home Office under the Animal [Scientific Procedures] Act 1986 license 70/8325. All mice were maintained under specific pathogen-free conditions in individually ventilated cages (Techniplast GM500, Techniplast) on Ligno-cel FS14 spruce bedding (IPS, Ltd.) with environmental enrichment (fun tunnel, chew stick, and Enviro-Dri nesting material (LBS)) at 19-23 °C with light from 7:00 a.m. to 7:00 p.m. and fed Dietex CRM pellets (Special Diet Services) *ad libitum*. No animals were wild and no field collected samples were used. Unless otherwise stated, mice were maintained on a C57BL/6J background. Embryos were used at various stages from E8.5-E18.5 as indicated in the text. Samples were collected from animals at 14 days postpartum or at 8-12 weeks as specified in the text. Females used in timed mating experiments were aged between 6 and 18 weeks. The investigators were blinded to the genotypes of animals throughout the study and data were acquired by relying purely on identification numbers. *Fanca*$^{tm1a(EUCOMM)Wtsi}$; MGI ID: 4434431, C57BL/6N, the conditional *Fanca*$^{tm1c(EUCOMM)Wtsi}$ allele, and the *Aldh2*$^{tm1a(EUCOMM)Wtsi}$; MGI: 4431566 allele have been described previously[54,58]. *Fan1*$^{tm1a(KOMP)Wtsi}$; MGI ID: 4940765, C57BL/6N/129S4 were a kind gift from F Hildebrandt[44]. *Xpa*^{tm1Gvh}; MGI ID: 5312129, C57BL/6 and *Ercc6*^{tm1Gvh} *(Csb)*; MGI ID: 1932102, C57BL/6 mice were a kind gift from G.T. van der Horst[69,70]. *Stella-GFP (Tg(Dppa3/EGFP)6-25Masu)*; MGI:5519126 mice were a kind gift from Azim Surani[19]. GOF18-*GFP (Tg(Pou5f1-EGFP)2Mnn)*; MGI:3057158; JAX:004654, and *Stra8-iCre (Tg(Stra8-icre)1Reb/J)*; MGI:3779079; Jax:008208 mice were purchased from the Jackson Laboratory.

Generation of *Ercc1*-deficient mice

Ercc1-mutant mice were generated from C57BL/6 ES cells (*Ercc1*$^{tm1a(KOMP)Wtsi}$;MGI: 4362172; Clone G12), carrying a targeted disruption of the *Ercc1* locus, obtained from the EUCOMM consortium. These mice were backcrossed onto a C57BL/6J background. Targeting was confirmed by long-range PCR at both the 5’ and 3’ using oligonucleotide pairs LAR3+Ercc1GF3, and RAF5+Ercc1GR3 respectively. Germline transmission was achieved and progeny were genotyped using ER1F2, ER1R1 and En2a oligonucleotides. This allele was made conditional by crossing with mice transgenic for the Flp-e recombinase[71] to generate the *Ercc1*$^{tm1c(KOMP)Wtsi}$ allele. Cre recombinase led to the excision of exon 5 resulting in the *Ercc1*$^{tm1d(KOMP)Wtsi}$ allele. The *Ercc1*$^{tm1d(KOMP)Wtsi}$ allele was determined by genotyping using PCR with ER1NF and ER1NR oligonucleotides. Sequence of oligonucleotides are provided in Supplementary Table 1.

Isolation and characterization of *Ercc1*$^{-/-}$ mouse embryonic fibroblasts

Timed matings were performed between *Ercc1* heterozygous mice and pregnant females were culled by cervical dislocation at E12.5. Primary MEF cultures were obtained and immortalized using the SV40 large T antigen as described previously[23]. Briefly, pBABE-SV40-Puro virus was produced using Plat-E cells (Cell Biolabs). 48 hours following transfection, the culture medium containing retroviruses was collected and passed through a 0.22 μm filter. The filtered retrovirus was mixed 1:1 with complete medium and supplemented with 4 $\mu g.ml^{-1}$ polybrene, the resulting infective medium was added to primary MEF cultures. Transformed clones were selected for 10 days using 3.5 $\mu g.ml^{-1}$ puromycin. Sensitivity to DNA-damaging agents was determined by seeding 500 transformed MEFs per well of a 96-well flat-bottom plate and exposed to mitomycin c (MMC) or ultraviolet (UV) irradiation. After 10 days of culture post-exposure the MTS cell viability reagent (Promega) was added and plates incubated at 37 °C for 4 hours, and absorbance at 492 nm was measured.

Histological analysis

Tissues were fixed in 10% neutral-buffered formalin for 24-36 hours and transferred to 70% ethanol. Fixed samples were embedded in paraffin and 4 μm sections cut, deparaffinized, rehydrated and stained with hematoxylin and eosin following standard methods. Images were captured using a Zeiss AxioPlan 2 microscope (Zeiss) and tissue architecture was scored blindly.

Immunohistochemistry

Sections of formalin-fixed paraffin-embedded samples were deparaffinized and rehydrated following standard methods. Slides were placed into antigen retrieval buffer (10 mM sodium citrate, pH 6.0) and boiled for 10 minutes. Slides were allowed to cool to room temperature before being washed three times in water for 5 minutes and then once in TBS, 0.1% w/v Tween-20 for 5 minutes. A large hydrophobic ring was drawn around the tissue and the samples incubated in blocking buffer (TBS, 5% v/v goat serum, 0.1% w/v Tween-20) for 1 hour at room temperature. Samples were incubated at 4 °C overnight with the following primary antibodies diluted in blocking buffer; anti-MVH 1:100 (Abcam, ab27591), anti-PLZF 1:200 (Santa Cruz Biotechnology, sc-28319), anti-ERCC1 1:50 (Cell Signaling Technology, D6G6) and anti-cleaved-Caspase 3 1:400 (Cell Signaling Technology, 9661). Slides were washed three times with TBS, 0.1% w/v Tween-20 and then incubated with the following secondary antibodies diluted in blocking buffer for 1 hour at room temperature; goat anti-mouse Alexa Fluor 488 1:500 (A11029, Life Technologies), goat anti-rabbit Alexa Fluor 594 1:1,000 (A11037, Life Technologies), swine anti-rabbit or anti-mouse HRP-conjugated immunoglobulins 1:200 (Dako). Afterwards, slides were washed three times in TBS, 0.1% w/v Tween-20 for 5 minutes. For fluorescence-based immunohistochemistry, slides were incubated with 0.5 $\mu g.ml^{-1}$ 4'-6-diamidino-2-phenylindole (DAPI) diluted in PBS for 10 minutes. Slides were then washed once in water and mounted with ProLong Gold antifade reagent (P36934, Molecular Probes) and coverslips placed on top of the slides and allowed to cure for 48 hours. Images were captured using a Zeiss LSM 780 confocal microscope (Zeiss). The frequency of MVH-positive cells was scored blindly. For HRP-

based immunohistochemistry, slides were incubated for 3 minutes with diaminobenzidine (Cell Signaling Technology, 8059P) and then washed once in water. Samples were counterstained with 50% hematoxylin diluted in water for 5 minutes. Afterwards slides were washed 2 times in water for 5 minutes and dehydrated in an ethanol gradient and finally xylene before being mounted with D.P.X (Sigma, 317616) and coverslips placed onto slides. Images were captured using a Zeiss AxioPlan 2 microscope (Zeiss). The frequency of PLZF-positive cells and presence of ERCC1 were scored blindly.

Preparation and spreading of meiotic cells

The spreading and staining of meiotic cells was performed as described previously with some modifications[33–37,72]. Briefly, the seminiferous tubules of 21-day old (P21) or 50-day old (P50) male mice or the ovaries of embryonic day 16.5 (E16.5) or 18.5 (E18.5) female fetuses were incubated in hypotonic extraction buffer (30 mM Tris, 50 mM sucrose, 17 mM trisodium citrate dehydrate, 5 mM ethylenediaminetetraacetic acid (EDTA), 0.5 mM Dithiothreitol (DTT) 0.5 mM phenylmethane sulfonyl fluoride, pH 8.2) for 1 hour at room temperature with gentle agitation. Samples were allowed to settle under gravity and the supernatant discarded. Samples were placed onto a glass slide and excess buffer removed. Samples were then disaggregated in 100 μl of 100 mM sucrose solution, pH 8.2, using a fine pair of forceps and a scalpel. The cell suspension was made up to a final volume of 200 μl (100 mM sucrose, pH 8.2), and dropped from a height of 0.5 m onto glass slides coated in 10 mM sodium borate, 1% w/v PFA, 0.15% w/v Triton X-100, pH 9.2. Slides were left to air dry for 2 hours before being washed three times in PBS for 5 minutes. Samples were blocked in PBS, 3% w/v BSA and 0.1% w/v Triton X-100 for 30 minutes at room temperature. The following primary antibodies were diluted in blocking buffer and incubated overnight at room temperature; anti-γ-H2A.X 1:1,000 (Millipore, JBW301) and anti-SCP3 1:300 (Santa Cruz Biotechnology, sc-33195). Slides are were washed three times in PBS, 0.1% w/v Triton X-100 for 5 minutes and incubated in the following secondary antibodies diluted in blocking buffer for 1 hour at room temperature; goat anti-mouse Alexa Fluor 488 (A11029, Life Technologies) and goat anti-rabbit Alexa Fluor 594 (A11037, Life Technologies). The slides were then washed three times in PBS, 0.1% w/v Triton X-100 for 5 minutes and stained with 0.5 μg.ml^{-1} DAPI diluted in PBS for 10 minutes. Slides were washed once in water and mounted with ProLong Gold antifade reagent (P36934, Molecular Probes) and coverslips placed on top of the slides. Images were captured using a Zeiss LSM 780 confocal microscope (Zeiss). The frequencies of meiotic intermediates were scored blindly following standard criteria.

Assessing the fertility of DNA-repair-deficient mice

To determine if mutant mice were capable of giving rise to offspring, test mice were paired with wildtype C57BL/6J mates of the opposite gender. Females were examined daily for the presence of copulation plugs. The numbers of pups born over three successive months were recorded (only mating pairs in which at least 3 copulation plugs were found were included in the final analysis). Individuals performing copulation plug checks were blinded to the genotype of mice.

Embryo isolation and fetal gonad dissection

Timed matings were performed overnight and female mice were assessed for the presence of copulation plugs the following day and separated from males. Halfway through the light cycle on the day a copulation plug was observed was designated E0.5. Pregnant mice were culled by cervical dislocation and exsanguination at noon of the appropriate day during gestation (E9.5-18.5) and the embryos harvested. Embryos were dissected and individual where appropriate fetal gonads placed into ice-cold PBS and further analysis performed immediately.

Whole-mount fluorescence imaging of fetal gonads

Gonads from developing embryos (E11.5-13.5) carrying the *GOF18-GFP* PGC reporter were dissected as previously described. Briefly, embryonic gonads were dissected and placed in ice-cold PBS and washed three times in ice-cold PBS. Whole-mount fluorescence images were acquired on a Leica DM IL inverted microscope (Leica) using a Lumen200 light source (Scitech).

Analysis of PGC distribution in whole-mount embryos

Embryos were harvested at E9.5, E10.5 and E11.5 following timed matings between *Ercc1* heterozygous mice carrying the *GOF18-GFP* reporter, as described previously. Embryos were fixed in 10% neutral-buffered formalin overnight at 4 °C and washed three times in PBS for five minutes each. In the case of E10.5 embryos the right body wall was dissected to reveal the genital ridge and placed on their left side and embedded in 1% w/v low melting point agarose. In the case of E11.5 embryos the front abdominal wall and visceral organs were dissected away to reveal the genital ridge[47] and embryos were placed ventral side down and embedded in 1% w/v low melting point agarose to facilitate visualization of GOF18-GFP^+ PGCs. Samples were incubated at 4 °C for 30 minutes, until the agarose had fully set. Whole-mount fluorescence images were acquired using an ECLIPSE TE2000 inverted epifluorescence microscope (NIKON). In the case of E10.5 embryos somites were used as physiological landmarks to assess the distribution of PGCs along the hindgut.

Quantification of PGCs *in vivo*

For PGC quantification, urogenital ridges of developing embryos (E11.5-13.5) or embryos (E9.5-10.5) carrying either the *GOF18-GFP* or *Stella-GFP* reporter were isolated and placed into 150 μl (or 500 μl in the case of E9.5-10.5 embryos) of trypsin solution (2.5 $\mu g.ml^{-1}$ trypsin (Gibco), 25 mM Tris, 120 mM NaCl, 25 mM KCl, 25 mM KH_2PO_4, 25 mM Glucose, 25 mM EDTA, pH 7.6) pre-warmed to 37 °C and incubated for 10 minutes at 37 °C. Subsequently 1 μl of Benzonase (EMD Millipore) was added and the sample disaggregated by gentle pipetting and incubated for a further 5 minutes at 37 °C. The trypsin was inactivated by the addition of 1 ml of PBS, 5% v/v fetal calf serum (FCS). Following 10 minutes of centrifugation at 3,300 r.p.m., the cell pellet was resuspended in 100 μl of Alexa Fluor 647-conjugated anti-human/mouse CD15 (SSEA1) (BioLegend, MC-480) diluted 1:100 in PBS, 2.5% v/v FCS and incubated at room temperature for 10 minutes. 300 μl of PBS, 2.5% v/v FCS was added to the cell suspension and the samples immediately run on an Eclipse analyzer (Sony Biotechnology Inc.) and the data analyzed using FlowJo v10.1r5.

Assessment of PGCs for DNA damage and DNA damage response markers

E11.5 fetal gonads were dissected as previously described and fixed in PBS, 4% w/v paraformaldehyde (PFA) for 30 minutes at 4 °C. Fixed gonads were then washed three times in PBS, 1% w/v Triton X-100 for 15 minutes at room temperature before being pressed onto glass slides and a hydrophobic circle drawn around the tissue. Slides were blocked in PBS, 1% w/v BSA, 1% w/v Triton X-100 for 30 minutes at room temperature before being incubated overnight at 4 °C with the following primary antibodies diluted in blocking buffer; anti-GFP 1:500 (Nacalai, GF090R), anti-γ-H2A.X 1:1,000 (Millipore, JBW301), anti-53BP1 1:1,000 (Novus, NB100-304), anti-cleaved Caspase-3 1:400 (Cell Signaling Technology, 9661), anti-phospho-p53 (Ser15) 1:500 (Cell Signaling Technology, D4S1H). Slides were then washed three times in PBS, 1% w/v Triton X-100 for 5 minutes and incubated with the following secondary antibodies diluted in blocking buffer, for 1 hour at room temperature; goat anti-rat Alexa Fluor 488 1:1,000 (A11006, Life Technologies), goat anti-mouse Alexa Fluor 594 1:1,000 (A11032, Life Technologies) and goat anti-rabbit Alexa Fluor 594 1:1,000 (A11037, Life Technologies). The slides were then washed three times in PBS, 1% w/v Triton X-100 for 5 minutes and stained with 0.5 $\mu g.ml^{-1}$ DAPI diluted in PBS for 10 minutes. Slides were washed once in water and mounted with ProLong Gold anti-fade reagent (P36934, Molecular Probes) and coverslips placed onto slides. Images were captured using a Zeiss LSM 780 confocal microscope (Zeiss). DNA damage foci per nucleus or staining of DNA damage response markers were scored blindly.

Isolation of primordial germ cells

For FACS sorting of PGCs (GOF18-GFP^+) and surrounding somatic cells (GOF18-GFP^-) individual gonads of developing embryos (E11.5-13.5) or whole embryos (E8.5-10.5) carrying the *GOF18-GFP* reporter were isolated as previously described and placed into pre-warmed trypsin solution (2.5 $\mu g.ml^{-1}$ trypsin (Gibco), 25 mM Tris, 120 mM NaCl, 25 mM KCl, 25 mM KH_2PO_4, 25 mM Glucose, 25 mM EDTA, pH 7.6) and incubated for 10 minutes at 37 °C. Subsequently 1 μl of Benzonase (EMD Millipore) was added and the sample disaggregated by pipetting and incubated for a further 5 minutes at 37 °C. The trypsin was inactivated by the addition of 1 ml of PBS, 5% v/v fetal calf serum (FCS). Following 10 minutes of centrifugation the cell pellet was resuspended in 100 μl of Alexa Fluor 647-conjugated anti-human/mouse CD15 (SSEA1) (BioLegend, MC-480) diluted 1:100 in PBS, 2.5% v/v FCS and incubated at room temperature for 10 minutes. 300 μl of PBS, 2.5% v/v FCS was added to the cell suspension and the samples passed through a 70 μm cell strainer. Samples were immediately run on a Synergy sorter (Sony Biotechnology Inc.) and the cells sorted into 10 μL PBS. Sorted PGCs were centrifuged at 13,000 r.p.m. in a centrifuge chilled to 4°C and the cell pellets stored at -80 °C until further analysis.

Quantitative RT-PCR and gene expression analysis

Primordial germ cells (GOF18-GFP^+) and surrounding somatic cells (GOF18-GFP^-) were isolated from E8.5-12.5 embryos carrying the *GOF18-GFP* reporter by FACS as described above. Total RNA was extracted using the PicoPure™ RNA Isolation kit (Life Technologies) and first strand cDNA was synthesized using the Superscript III reverse transcriptase (Life Technologies) following the manufacturer's instructions. Quantitative real-time PCR

analysis for the expression of *Ap2γ, Prdm14, Blimp-1, Stella, Mvh* and *Dazl* was performed using oligonucleotides described previously[45,46]. qPCR was performed using Brilliant II SYBR® Green QPCR Master Mix (Invitrogen) in a Viia7 (ThermoFisher) cycler at 95 °C for 10 minutes and 40 cycles of 95 °C for 15 seconds and 60 °C for 1 minute. Mean threshold cycles were determined from 3 technical repeats using the comparative CT methodology. All expression levels were normalised to *Gapdh*. Taqman probes were used for qRT-PCR expression analysis of *Ercc1* (m00468337_m1), *Xpa* (mm00457111_m1), *Fanca* (mm01243361_g1), Plzf (mm01176868_m1) and *Stella* (mm01184198_g1) PCR amplification was performed using the TaqMan Fast Advanced Master Mix (ThermoFisher Scientific). PCR amplification was performed on a Viaa7 cycler for 95 °C for 15 seconds and 60°C for 1 minute. Mean threshold cycles were determined from 3 technical repeats using the comparative CT methodology. All expression levels were normalized to *Gapdh* (mm99999915_g1).

Bisulfite Sequencing

Primordial germ cells (GOF18-GFP$^+$) and surrounding somatic cells (GOF18-GFP$^-$) were purified from E12.5 embryos carrying the *GOF18-GFP* reporter by FACS as previously described. Genomic DNA extraction and bisulfite conversion was performing using the EZ DNA Methylation-Direct™ Kit (Zymo Research) following the manufacturer's instructions. Nested primer pairs were used to amplify the following genomic regions using the ZymoTaq™ polymerase (Zymo Research). The oligonucleotides used to amplify *Mili*[46], *Tex19.1*[46], *H19DMR*[73], and *Line1*[52] were described previously. PCR products were ran out on an agarose gel and a single-band excised, gel-extracted using the QIAquick® Gel Extraction Kit (QIAGEN) following manufacturer's instructions and cloned into the pGEM-T Easy Vector System I (Promega) for sequencing. Sequencing reads were analyzed using the free online software quantification tool for methylation analysis (QUMA) using standard quality control settings.

Single-cell gel electrophoresis (Comet assay)

Primordial germ cells (GOF18-GFP$^+$) were purified from E11.5 embryos carrying the *GOF18-GFP* reporter by FACS as previously described. Purified PGCs were sorted into PBS at a concentration of 100,000 cells per ml and were mixed with molten low melting point agarose (LMAgarose), which was boiled and then equilibrated to 37 °C at 1:10 v/v: LMAgarose). 50 μl of cell suspension (1 part cell solution 10 parts molten LMAgarose) was added to each well of a 2-well CometSlide™ (Trevigen®) to form a thin, uniform layer and allowed to set for 30 minutes at 4°C in the dark. Samples were lysed overnight at in pre-chilled lysis solution (Trevigen®) at 4 °C in the dark. Samples were drained and incubated in pre-chilled alkaline unwinding solution (200 mM NaOH, 1 mM EDTA, pH > 13) for 1 hour at 4 °C. Slides were transferred to an electrophoresis tank containing alkaline electrophoresis solution (200 mM NaOH, 1 mM EDTA, pH > 13) and 1 volt/cm was applied for 30 minutes, as described in the manufacturer's instructions. Slides were drained and washed twice in water for 5 minutes each before being placed into 70% ethanol for a further 5 minutes. Slides were then dried at 37 °C in the dark for 10 minutes. Comets were stained with 100 μl of 1:10,000 (v/v) SYBR™ gold nuclei acid stain (Invitrogen) for 30 minutes at RT in the dark. Comets were imaged by epifluorescence microscopy using a Zeiss AxioPlan 2

microscope (Zeiss) and comet tail moment was calculated using the CometScore software (TriTek).

Derivation, maintenance and gene targeting of mouse embryonic stem cells

Wildtype and *Fanca*$^{-/-}$ mouse embryonic stem cells (mESCs) were derived from mice carrying the *GOF18-GFP* reporter. Pluripotent mESCs were maintained in N2B27 media supplemented with the Glycogen synthase kinase-3 inhibitor, CHIR99021 (Axon Medchem, 1386), the MAPK/ERK inhibitor PD0325901 (Axon Medchem, 1408), and mouse leukemia inhibitory factor (LIF) (Cambridge Stem Cell Institute) referred to as to 2i + LIF media. *Ercc1*$^{-/-}$ *GOF18-GFP* mESCs were generated by transfecting wildtype mESCs with px461 containing the Cas9 (D10A) and the guides mmErcc1Nicka and mmErcc1Nickb. Sequence of oligonucleotides are provided in Supplementary Table 1. Whole mESC lysates were probed using the anti-ERCC1 (Santa Cruz Biotechnology, sc-1708) primary antibody as described previously and successfully targeted clones expanded. This resulted in a homozygous deletion of 59bp in the *Ercc1* locus resulting in transcripts containing a frameshift.

Generation and quantification of PGCLCs *in vitro*

Wildtype, *Ercc1*$^{-/-}$ and *Fanca*$^{-/-}$ mESCs carrying the *GOF18-GFP* reporter were maintained as previously described and differentiated into primordial germ cell-like cells (PGCLCs) as described previously[38]. To determine the frequency of PGCLCs generated from mESCs, PGCLC colonies were harvested by centrifugation at 3,300 r.p.m. for 10 minutes and cell pellets resuspended in 500 μl of pre-warmed trypsin solution and incubated for 10 minutes at 37 °C. Afterwards, 1 μl of Benzonase (EMD Millipore) was added and the samples disaggregated by pipetting and incubated for a further 5 minutes at 37 °C. The trypsin was inactivated by the addition of 1 ml of PBS, 5% v/v FCS. Following 10 minutes of centrifugation at 3,300 r.p.m., the cell pellet was resuspended in 100 μl of Alexa Fluor 647-conjugated anti-human/mouse CD15 (SSEA1) (BioLegend, MC-480) diluted 1:100 in PBS, 2.5% v/v FCS and incubated at room temperature for 10 minutes. The cell suspension was diluted by added 300 μl of PBS, 2.5% v/v FCS and the frequency of PGCLCs (SSEA1^{+}GFP^{+}) determined by flow cytometric analysis on a BD LSRFortessa analyser (BD Biosciences) and the data analyzed using FlowJo v10.1r5.

Western Immunoblotting

Unless otherwise stated the following primary antibodies were used for western immunoblotting, diluted in 5% w/v BSA, 0.1% Tween-20 TBS and incubated at 4 °C overnight with gentle agitation; Anti-ERCC1 antibody 1:100 (Santa Cruz Biotechnology, sc-1708), anti-FANCA 1:1,000 (Cell Signaling Technology, D1L2Z), anti-PLZF 1:100 (Santa Cruz Biotechnology, sc-28319), anti-Histone H3 1:5,000 (Abcam, 1791), anti-β-ACTIN 1:3,000 (Abcam, 8227), anti-VINCULLIN 1:2,000 (Abcam, 129002). The following secondary antibodies were diluted in 5% w/v BSA, 0.1% Tween-20 TBS and incubated for 1 hour at room temperature with gentle agitation; Swine anti-rabbit or anti-mouse HRP-conjugated immunoglobulins 1:2,000 (Dako). To demonstrate the absence of ERCC1 in *Ercc1*-mutant MEFs derived from *Ercc1*$^{tm1a(KOMP)Wtsi}$ embryos anti-ERCC1 1:1,000 (Cell

Signaling Technology, D6G6) was employed, following the same western immunoblotting protocol described previously.

Cell cycle analysis following EdU incorporation

To assess the incorporation of EdU into the DNA of PGCs in vivo, pregnant mice were given a single dose of 50 mg/kg EdU by intraperitoneal (IP) injection at 10 ml/kg. Following a 1 hour incubation period the female was sacrificed by cervical dislocation and the fetal gonads of E11.5 embryos were harvested. Following a 1 hour incubation period the fetal gonads of E11.5 embryos were harvested as previously described and placed into 150 μl pre-warmed trypsin and incubated for 10 minutes at 37 °C. Subsequently 1 μl of Benzonase (EMD Millipore) was added and the colonies disaggregated by pipetting and incubated for a further 5 minutes at 37 °C. Trypsin was inactivated by the addition of 1 ml of PBS, 5% v/v FCS. Following 10 minutes of centrifugation at 3,300 r.p.m., the cell pellet was re-suspended in 100 μl of Alexa Fluor 647-conjugated anti-human/mouse CD15 (SSEA-1) (BioLegend, MC-480) diluted 1:100 in PBS, 2.5% v/v FCS and incubated at room temperature for 10 minutes. 1 ml of PBS, 2.5% v/v FCS was added and the samples centrifuged at 3,300 r.p.m. After centrifugation the samples were re-suspended in 100 μl of IntraPrep fixative reagent (A07803, Beckman Coulter) and incubated at room temperature for 15 minutes. 1 ml of PBS, 5% FCS was added the samples and centrifuged at 3,300 r.p.m. Cell pellets were then re-suspended in 100 μl of IntraPrep permeabilisation buffer (A07803, Beckman Coulter) and incubated at room temperature whilst the Click-iT® azide solution (C10646, Invitrogen) is prepared (following the manufacturer's instructions). 500 μl of Alexa Fluor 594 picolyl azide solution is added to each sample and incubated at room temperature for 30 minutes. 1 ml of saponin solution (C10646, Invitrogen) is added before the samples are centrifuged at 3,300 r.p.m. Samples are resuspended in 500 μl of PBS, 2.5% v/v FCS, 0.5 $\mu g.ml^{-1}$ DAPI and incubated at room temperature for 10 minutes. The samples were analyzed immediately on a BD LSRFortessa (BD Biosciences) analyzer and the data analyzed using FlowJo v10.1r5.

Immunoblotting of spermatogonial stem cells

To assess the success of *Stra8-iCre*-mediated disruption of the conditional *Ercc1* and *Fanca* alleles, spermatogonial stem cells were sorted from adult testes for western blot analysis, essentially as described previously[74]. Briefly, 8- to 12-week old mice were culled by cervical dislocation, the testes dissected and tunica albuginea removed. Decapsulated testes were incubated in 3.5 ml Gey's balanced salt solution (GBSS) (Sigma, G9779) containing 120 $units.ml^{-1}$ collagenase type I (Sigma, SCR103) and 10 μl of DNase I (Sigma, DN25) stock solution (1 $mg.ml^{-1}$) and incubated at 55 °C for 15 minutes with gentle agitation. The testicular tubules were allowed to settle under gravity and the supernatant discarded, and the process repeated once more. Following the aspiration of the second supernatant, samples were incubated in 2.5 ml GBSS containing 120 $units.ml^{-1}$ collagenase type I, 1 $mg.ml^{-1}$ trypsin and 10 μl DNase I for 15 minutes at 55 °C with gentle agitation. After gentle disaggregation using a Pasteur pipette samples were stained with Hoechst 33342 (Life Technology, H3570) added to a final concentration 350 $ug.ml^{-1}$. The samples were run on a Synergy sorter (Sony Biotechnology Inc.) with 5 $ug.ml^{-1}$ propidium iodide. Viable spermatogonia, defined as PI-negative, Hoechst red low and Hoechst blue low, were sorted

into 500 μl PBS. Sorted spermatogonia were centrifuged at 13,000 r.p.m. in a centrifuge chilled to 4 °C and the cell pellets lysed in SDS-PAGE running buffer (Thermo Fisher Scientific, NP0008). Whole cell lysates of 100,000 spermatogonial stem cells were immunoblotted for ERCC1 or FANCA using the anti-ERCC1 antibody 1:100 (Santa Cruz Biotechnology, sc-1708) and the anti-FANCA antibody 1:1,000 (Cell Signaling Technology, D1L2Z) as previously described.

Statistical analysis

The number of independent biological samples and technical repeats (*n*) are indicated in figure legends. Unless otherwise stated data are shown as mean ± standard error of the mean (s.e.m.) and the nonparametric Mann-Whitney test was employed to determine statistical significant. Analysis was performed in GraphPad Prism version 8.

Supplementary Material

Refer to Web version on PubMed Central for supplementary material.

Acknowledgements

We would like to thank The Wellcome Trust Sanger Institute, the KOMP Consortium, and the Mouse Biology Program (MBP) University of California for *Ercc1*-targeted mESCs. We thank Azim Surani for the gift of *Stella-GFP* mice, F. Hildebrandt for *Fan1*-deficient mice, G.T. van der Horst for the gift of XPA- and CSB-deficient mice. We would like to thank K.J. Patel for ALDH2- and ADH5-deficient mice. We thank the Human Research Tissue Bank (NIHR Cambridge Biomedical Research Centre) for processing histology. We would like to thank Richard Pannell, Claire Knox, Chloe Watson, Kirsty Kemp, Rob Higginson, Jess Clark, the Ares and Biomed staff for assistance with animal procedures and experiments. We thank Maria Daly, Fan Zhang and the Flow Cytometry Core staff for technical assistance. We would like to thank Gonçalo Oliveira for assistance with PGCLC assays. We would like to thank Juan Garaycoechea for criticism, screening *Ercc1* founder mice, for collecting samples from NER-deficient mice, and for critically reading the manuscript. We would like to thank Julian Sale for critically reading the manuscript and for useful discussions. R.J.H. and G.P.C. are supported by Medical Research Council. This work was supported by the Medical Research Council, as part of United Kingdom Research and Innovation (also known as UK Research and Innovation) [MRC file reference number MC_UP_1201/18]. G.P.C. would like to thank K.J. Patel for scientific discussion and support.

References

1. Veltman JA, Brunner HG. De novo mutations in human genetic disease. Nat Rev Genet. 2012; 13:565–75. [PubMed: 22805709]
2. Tang WW, Kobayashi T, Irie N, Dietmann S, Surani MA. Specification and epigenetic programming of the human germ line. Nat Rev Genet. 2016; 17:585–600. [PubMed: 27573372]
3. Hajkova P, et al. Genome-wide reprogramming in the mouse germ line entails the base excision repair pathway. Science. 2010; 329:78–82. [PubMed: 20595612]
4. Surani MA, Durcova-Hills G, Hajkova P, Hayashi K, Tee WW. Germ line, stem cells, and epigenetic reprogramming. Cold Spring Harb Symp Quant Biol. 2008; 73:9–15. [PubMed: 19022742]
5. Hajkova P, et al. Chromatin dynamics during epigenetic reprogramming in the mouse germ line. Nature. 2008; 452:877–81. [PubMed: 18354397]
6. Nik-Zainal S, et al. Mutational processes molding the genomes of 21 breast cancers. Cell. 2012; 149:979–93. [PubMed: 22608084]
7. Alexandrov LB, Nik-Zainal S, Wedge DC, Campbell PJ, Stratton MR. Deciphering signatures of mutational processes operative in human cancer. Cell Rep. 2013; 3:246–59. [PubMed: 23318258]
8. Alexandrov LB, et al. Signatures of mutational processes in human cancer. Nature. 2013; 500:415–21. [PubMed: 23945592]

9. Sekelsky JJ, McKim KS, Chin GM, Hawley RS. The Drosophila meiotic recombination gene mei-9 encodes a homologue of the yeast excision repair protein Rad1. Genetics. 1995; 141:619–27. [PubMed: 8647398]
10. Yildiz O, Majumder S, Kramer B, Sekelsky JJ. Drosophila MUS312 interacts with the nucleotide excision repair endonuclease MEI-9 to generate meiotic crossovers. Mol Cell. 2002; 10:1503–9. [PubMed: 12504024]
11. Saito TT, Lui DY, Kim HM, Meyer K, Colaiacovo MP. Interplay between structure-specific endonucleases for crossover control during Caenorhabditis elegans meiosis. PLoS Genet. 2013; 9:e1003586. [PubMed: 23874210]
12. Baker BS, Carpenter AT. Genetic analysis of sex chromosomal meiotic mutants in Drosophilia melanogaster. Genetics. 1972; 71:255–86. [PubMed: 4625747]
13. Hsia KT, et al. DNA repair gene Ercc1 is essential for normal spermatogenesis and oogenesis and for functional integrity of germ cell DNA in the mouse. Development. 2003; 130:369–78. [PubMed: 12466203]
14. McWhir J, Selfridge J, Harrison DJ, Squires S, Melton DW. Mice with DNA repair gene (ERCC-1) deficiency have elevated levels of p53, liver nuclear abnormalities and die before weaning. Nat Genet. 1993; 5:217–24. [PubMed: 8275084]
15. Niedernhofer LJ, et al. A new progeroid syndrome reveals that genotoxic stress suppresses the somatotroph axis. Nature. 2006; 444:1038–43. [PubMed: 17183314]
16. Buaas FW, et al. Plzf is required in adult male germ cells for stem cell self-renewal. Nat Genet. 2004; 36:647–52. [PubMed: 15156142]
17. Szabo PE, Hubner K, Scholer H, Mann JR. Allele-specific expression of imprinted genes in mouse migratory primordial germ cells. Mech Dev. 2002; 115:157–60. [PubMed: 12049782]
18. Yeom YI, et al. Germline regulatory element of Oct-4 specific for the totipotent cycle of embryonal cells. Development. 1996; 122:881–94. [PubMed: 8631266]
19. Payer B, et al. Generation of stella-GFP transgenic mice: a novel tool to study germ cell development. Genesis. 2006; 44:75–83. [PubMed: 16437550]
20. Ohinata Y, et al. Blimp1 is a critical determinant of the germ cell lineage in mice. Nature. 2005; 436:207–13. [PubMed: 15937476]
21. Ahmad A, et al. ERCC1-XPF endonuclease facilitates DNA double-strand break repair. Mol Cell Biol. 2008; 28:5082–92. [PubMed: 18541667]
22. Bogliolo M, et al. Mutations in ERCC4, encoding the DNA-repair endonuclease XPF, cause Fanconi anemia. Am J Hum Genet. 2013; 92:800–6. [PubMed: 23623386]
23. Crossan GP, et al. Disruption of mouse Slx4, a regulator of structure-specific nucleases, phenocopies Fanconi anemia. Nat Genet. 2011; 43:147–52. [PubMed: 21240276]
24. Kottemann MC, Smogorzewska A. Fanconi anaemia and the repair of Watson and Crick DNA crosslinks. Nature. 2013; 493:356–63. [PubMed: 23325218]
25. Wong JC, et al. Targeted disruption of exons 1 to 6 of the Fanconi Anemia group A gene leads to growth retardation, strain-specific microphthalmia, meiotic defects and primordial germ cell hypoplasia. Hum Mol Genet. 2003; 12:2063–76. [PubMed: 12913077]
26. Sklavos MM, Giri N, Stratton P, Alter BP, Pinto LA. Anti-Mullerian hormone deficiency in females with Fanconi anemia. J Clin Endocrinol Metab. 2014; 99:1608–14. [PubMed: 24438373]
27. Giri N, Stratton P, Savage SA, Alter BP. Pregnancies in patients with inherited bone marrow failure syndromes in the NCI cohort. Blood. 2017; 130:1674–1676. [PubMed: 28838890]
28. Alavattam KG, et al. Elucidation of the Fanconi Anemia Protein Network in Meiosis and Its Function in the Regulation of Histone Modifications. Cell Rep. 2016; 17:1141–1157. [PubMed: 27760317]
29. Agoulnik AI, et al. A novel gene, Pog, is necessary for primordial germ cell proliferation in the mouse and underlies the germ cell deficient mutation, gcd. Hum Mol Genet. 2002; 11:3047–53. [PubMed: 12417526]
30. Luo Y, et al. Hypersensitivity of primordial germ cells to compromised replication-associated DNA repair involves ATM-p53-p21 signaling. PLoS Genet. 2014; 10:e1004471. [PubMed: 25010009]

31. Houghtaling S, et al. Epithelial cancer in Fanconi anemia complementation group D2 (Fancd2) knockout mice. Genes Dev. 2003; 17:2021–35. [PubMed: 12893777]
32. Yang Y, et al. Targeted disruption of the murine Fanconi anemia gene, Fancg/Xrcc9. Blood. 2001; 98:3435–40. [PubMed: 11719385]
33. Newkirk SJ, et al. Intact piRNA pathway prevents L1 mobilization in male meiosis. Proc Natl Acad Sci U S A. 2017; 114:E5635–E5644. [PubMed: 28630288]
34. Long J, et al. Telomeric TERB1-TRF1 interaction is crucial for male meiosis. Nat Struct Mol Biol. 2017; 24:1073–1080. [PubMed: 29083416]
35. Yuen BT, Bush KM, Barrilleaux BL, Cotterman R, Knoepfler PS. Histone H3.3 regulates dynamic chromatin states during spermatogenesis. Development. 2014; 141:3483–94. [PubMed: 25142466]
36. Gaysinskaya V, Soh IY, van der Heijden GW, Bortvin A. Optimized flow cytometry isolation of murine spermatocytes. Cytometry A. 2014; 85:556–65. [PubMed: 24664803]
37. Larson EL, Keeble S, Vanderpool D, Dean MD, Good JM. The Composite Regulatory Basis of the Large X-Effect in Mouse Speciation. Mol Biol Evol. 2017; 34:282–295. [PubMed: 27999113]
38. Hayashi K, Ohta H, Kurimoto K, Aramaki S, Saitou M. Reconstitution of the mouse germ cell specification pathway in culture by pluripotent stem cells. Cell. 2011; 146:519–32. [PubMed: 21820164]
39. Hayashi K, et al. Offspring from oocytes derived from in vitro primordial germ cell-like cells in mice. Science. 2012; 338:971–5. [PubMed: 23042295]
40. von Meyenn F, et al. Comparative Principles of DNA Methylation Reprogramming during Human and Mouse In Vitro Primordial Germ Cell Specification. Dev Cell. 2016; 39:104–115. [PubMed: 27728778]
41. Seisenberger S, et al. The dynamics of genome-wide DNA methylation reprogramming in mouse primordial germ cells. Mol Cell. 2012; 48:849–62. [PubMed: 23219530]
42. Hodskinson MR, et al. Mouse SLX4 is a tumor suppressor that stimulates the activity of the nuclease XPF-ERCC1 in DNA crosslink repair. Mol Cell. 2014; 54:472–84. [PubMed: 24726326]
43. Trujillo JP, et al. On the role of FAN1 in Fanconi anemia. Blood. 2012; 120:86–9. [PubMed: 22611161]
44. Airik R, et al. A FANCD2/FANCI-Associated Nuclease 1-Knockout Model Develops Karyomegalic Interstitial Nephritis. J Am Soc Nephrol. 2016; 27:3552–3559. [PubMed: 27026368]
45. Gillich A, et al. Epiblast stem cell-based system reveals reprogramming synergy of germline factors. Cell Stem Cell. 2012; 10:425–39. [PubMed: 22482507]
46. Hackett JA, et al. Promoter DNA methylation couples genome-defence mechanisms to epigenetic reprogramming in the mouse germline. Development. 2012; 139:3623–32. [PubMed: 22949617]
47. Francis RJ, Lo CW. Primordial germ cell deficiency in the connexin 43 knockout mouse arises from apoptosis associated with abnormal p53 activation. Development. 2006; 133:3451–60. [PubMed: 16887824]
48. Takeuchi Y, Molyneaux K, Runyan C, Schaible K, Wylie C. The roles of FGF signaling in germ cell migration in the mouse. Development. 2005; 132:5399–409. [PubMed: 16291796]
49. Molyneaux KA, et al. The chemokine SDF1/CXCL12 and its receptor CXCR4 regulate mouse germ cell migration and survival. Development. 2003; 130:4279–86. [PubMed: 12900445]
50. Seki Y, et al. Extensive and orderly reprogramming of genome-wide chromatin modifications associated with specification and early development of germ cells in mice. Dev Biol. 2005; 278:440–58. [PubMed: 15680362]
51. Seki Y, et al. Cellular dynamics associated with the genome-wide epigenetic reprogramming in migrating primordial germ cells in mice. Development. 2007; 134:2627–38. [PubMed: 17567665]
52. Hajkova P, et al. Epigenetic reprogramming in mouse primordial germ cells. Mech Dev. 2002; 117:15–23. [PubMed: 12204247]
53. Olek A, Walter J. The pre-implantation ontogeny of the H19 methylation imprint. Nat Genet. 1997; 17:275–6. [PubMed: 9354788]
54. Garaycoechea JI, et al. Genotoxic consequences of endogenous aldehydes on mouse haematopoietic stem cell function. Nature. 2012; 489:571–5. [PubMed: 22922648]

55. Pontel LB, et al. Endogenous Formaldehyde Is a Hematopoietic Stem Cell Genotoxin and Metabolic Carcinogen. Mol Cell. 2015; 60:177–88. [PubMed: 26412304]
56. Langevin F, Crossan GP, Rosado IV, Arends MJ, Patel KJ. Fancd2 counteracts the toxic effects of naturally produced aldehydes in mice. Nature. 2011; 475:53–8. [PubMed: 21734703]
57. Rosado IV, Langevin F, Crossan GP, Takata M, Patel KJ. Formaldehyde catabolism is essential in cells deficient for the Fanconi anemia DNA-repair pathway. Nat Struct Mol Biol. 2011; 18:1432–4. [PubMed: 22081012]
58. Garaycoechea JI, et al. Alcohol and endogenous aldehydes damage chromosomes and mutate stem cells. Nature. 2018; 553:171–177. [PubMed: 29323295]
59. Lai CL, et al. Dominance of the inactive Asian variant over activity and protein contents of mitochondrial aldehyde dehydrogenase 2 in human liver. Alcohol Clin Exp Res. 2014; 38:44–50. [PubMed: 23909789]
60. Heyer BS, MacAuley A, Behrendtsen O, Werb Z. Hypersensitivity to DNA damage leads to increased apoptosis during early mouse development. Genes Dev. 2000; 14:2072–84. [PubMed: 10950870]
61. Raya A, et al. Disease-corrected haematopoietic progenitors from Fanconi anaemia induced pluripotent stem cells. Nature. 2009; 460:53–9. [PubMed: 19483674]
62. Muller LU, et al. Overcoming reprogramming resistance of Fanconi anemia cells. Blood. 2012; 119:5449–57. [PubMed: 22371882]
63. Takahashi K, Yamanaka S. Induction of pluripotent stem cells from mouse embryonic and adult fibroblast cultures by defined factors. Cell. 2006; 126:663–76. [PubMed: 16904174]
64. Kim S, et al. PRMT5 protects genomic integrity during global DNA demethylation in primordial germ cells and preimplantation embryos. Mol Cell. 2014; 56:564–79. [PubMed: 25457166]
65. Popp I, et al. Fanconi anemia with sun-sensitivity caused by a Xeroderma pigmentosum-associated missense mutation in XPF. BMC Med Genet. 2018; 19:7. [PubMed: 29325523]
66. Auerbach AD. Fanconi anemia and its diagnosis. Mutat Res. 2009; 668:4–10. [PubMed: 19622403]
67. Norris PG, Hawk JL, Avery JA, Giannelli F. Xeroderma pigmentosum complementation group F in a non-Japanese patient. J Am Acad Dermatol. 1988; 18:1185–8. [PubMed: 3372781]
68. Fujiwara Y, et al. Xeroderma pigmentosum groups C and F: additional assignments and a review of the subjects in Japan. J Radiat Res. 1985; 26:443–9. [PubMed: 3834095]
69. van der Horst GT, et al. Defective transcription-coupled repair in Cockayne syndrome B mice is associated with skin cancer predisposition. Cell. 1997; 89:425–35. [PubMed: 9150142]
70. Jaarsma D, et al. Age-related neuronal degeneration: complementary roles of nucleotide excision repair and transcription-coupled repair in preventing neuropathology. PLoS Genet. 2011; 7:e1002405. [PubMed: 22174697]
71. Farley FW, Soriano P, Steffen LS, Dymecki SM. Widespread recombinase expression using FLPeR (flipper) mice. Genesis. 2000; 28:106–10. [PubMed: 11105051]
72. Peters AH, Plug AW, van Vugt MJ, de Boer P. A drying-down technique for the spreading of mammalian meiocytes from the male and female germline. Chromosome Res. 1997; 5:66–8. [PubMed: 9088645]
73. Kawasaki Y, et al. Active DNA demethylation is required for complete imprint erasure in primordial germ cells. Sci Rep. 2014; 4
74. Getun IV, Torres B, Bois PR. Flow cytometry purification of mouse meiotic cells. J Vis Exp. 2011

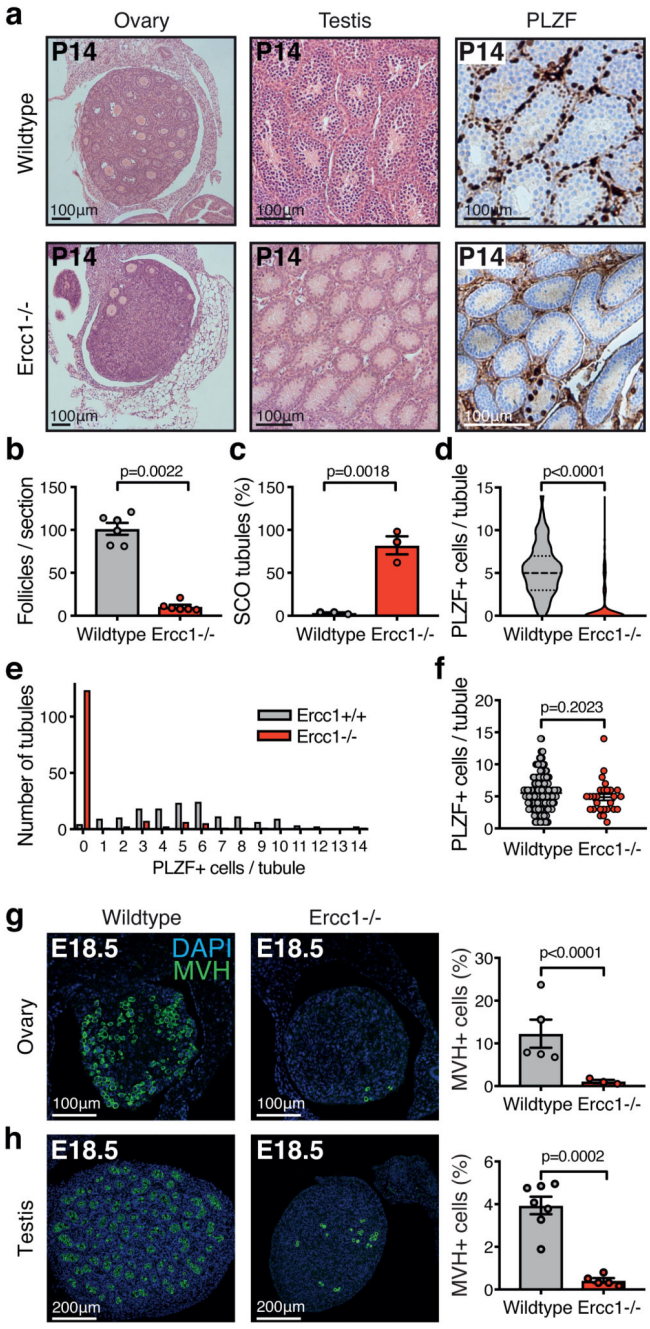

Figure 1. *Ercc1*$^{-/-}$ mice have reduced numbers of germ cells.

a, Hematoxylin and eosin (H&E)-stained sections of ovaries and H&E- and PLZF(brown)-stained sections of testes at 14 days of age (P14). **b**, Quantification of follicles per section of P14 ovary (*P* value calculated by 2-tailed Mann-Whitney test; data represent mean and s.e.m.; $n = 6$ independent animals per genotype). **c**, Frequency of Sertoli-cell-only (SCO) tubules per testis at P14 (*P* value calculated by 2-tailed Mann-Whitney test; data represent mean and s.e.m.; $n = 3$ independent animals per genotype). **d,** Quantification and distribution (**e**) of PLZF^{+} cells per seminiferous tubule at P14 (*P* value calculated by 2-tailed Mann-

Europe PMC Funders Author Manuscripts

Whitney test; data shown represent median and interquartile range; $n = 150$ tubules per genotype, 50 per mouse). **f**, Frequency of $PLZF^+$ cells per seminiferous tubule excluding tubules with no $PLZF^+$ cells in P14 mice (*P* value calculated by 2-tailed Mann-Whitney test; data shown represent mean and s.e.m.; $n = 150$ tubules per genotype, 50 per mouse). **g**, Representative images of E18.5 ovaries stained for the germ cell marker mouse vasa homologue (MVH) and the frequency of MVH^+ cells (*P* value calculated by 2-tailed Mann-Whitney test; data shown represent mean and s.e.m.;, each point represents data from one embryo, $n = 5$ and 3, left to right). **h**, Representative images of E18.5 testes stained for MVH and the frequency of MVH^+ cells (*P* value calculated by 2-tailed Mann-Whitney test; data shown represent mean and s.e.m.; each point represents data from one embryo, $n = 7$ and 5, left to right).

Europe PMC Funders Author Manuscripts

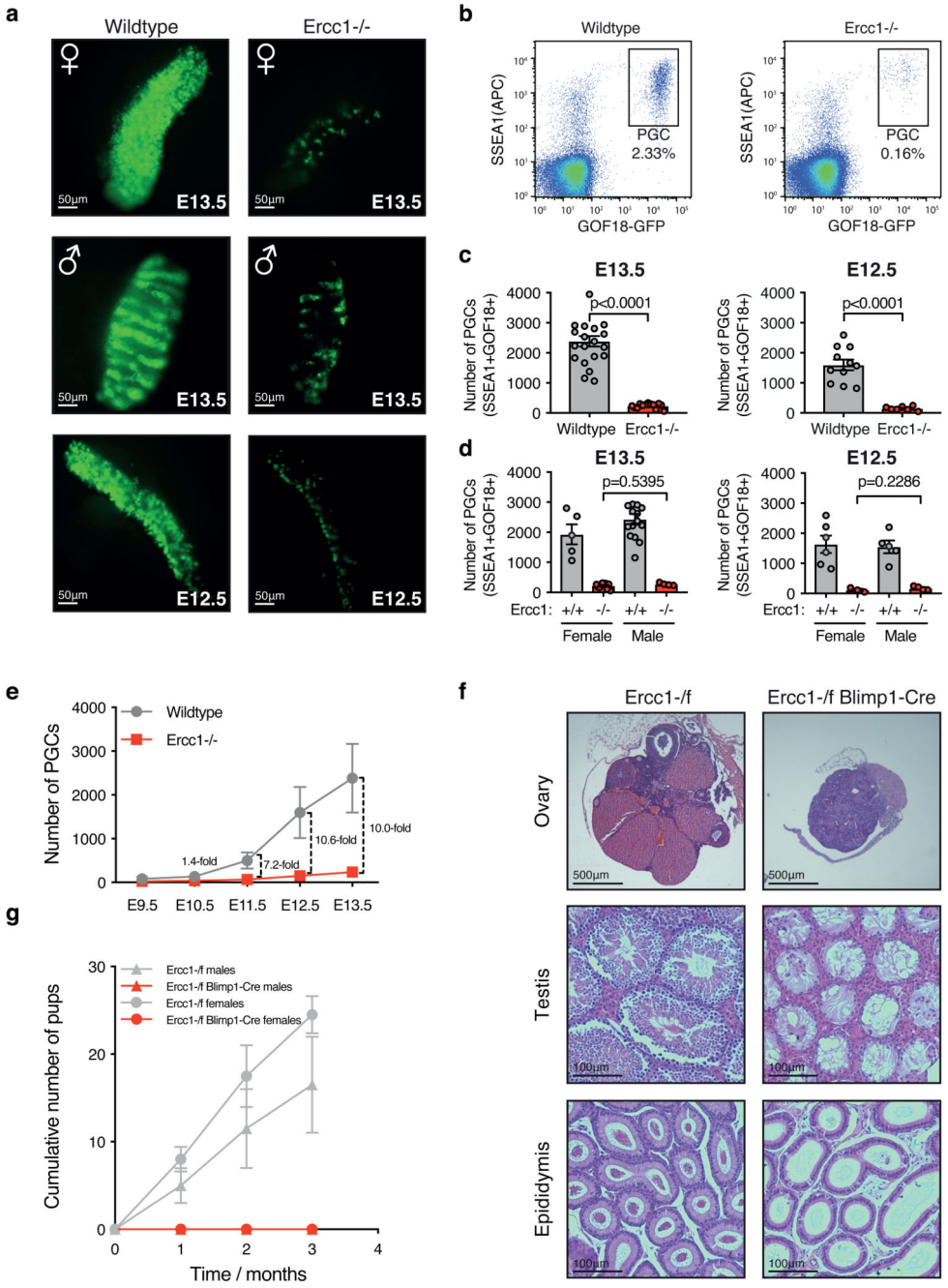

Figure 2. ERCC1 is critical for primordial germ cell development.

a, GOF18-GFP fluorescence in E13.5 (male and female) and E12.5 gonads from wildtype and *Ercc1*$^{-/-}$ embryos carrying the *GOF18-GFP* PGC reporter. **b**-**c**, Quantification of PGCs (GOF18-GFP^{+}SSEA1^{+}) by flow cytometry from wildtype and *Ercc1*$^{-/-}$ embryos at E13.5 and E12.5 (*P* value calculated by 2-tailed Mann-Whitney test; data shown represent mean and s.e.m.; each point represents data from one embryo, E13.5 $n = 19$ and 14, E12.5 $n = 11$ and 7, left to right, Gating strategy shown in Supplementary Fig. 18.) **d**, PGC number separated by sex at E13.5 and E12.5 (*P* value calculated by 2-tailed Mann-Whitney test; data

shown represent and s.e.m.; each point represents data from one embryo, E13.5 $n = 5$, 10, 15, and 4, E12.5 $n = 6$, 3, 5, and 4, left to right). **e**, Quantification of PGCs (GOF18-GFP $^{+}$SSEA1^{+}) throughout embryonic development (E9.5-13.5) in wildtype and *Ercc1*$^{-/-}$ embryos (data represent mean and s.e.m.; wildtype n =14, 10, 5, 11 and 21, *Ercc1*$^{-/-}$ $n = 6$, 7, 4, 7 and 14 embryos, left to right.). **f**, H&E-stained histology from 8-12 week old *Ercc1*$^{-/f}$ mice carrying *Blimp1-Cre* (similar results were obtained from 3 independent animals per genotype and gender). **g**, Quantification of the cumulative number of offspring over time when male or female *Ercc1*$^{-/f}$*Blimp1-Cre*$^{+}$ mice or controls were mated with wildtype mice and checked for evidence of copulation (data shown represent mean and s.e.m.; $n = 3$ mice per genotype).

Europe PMC Funders Author Manuscripts

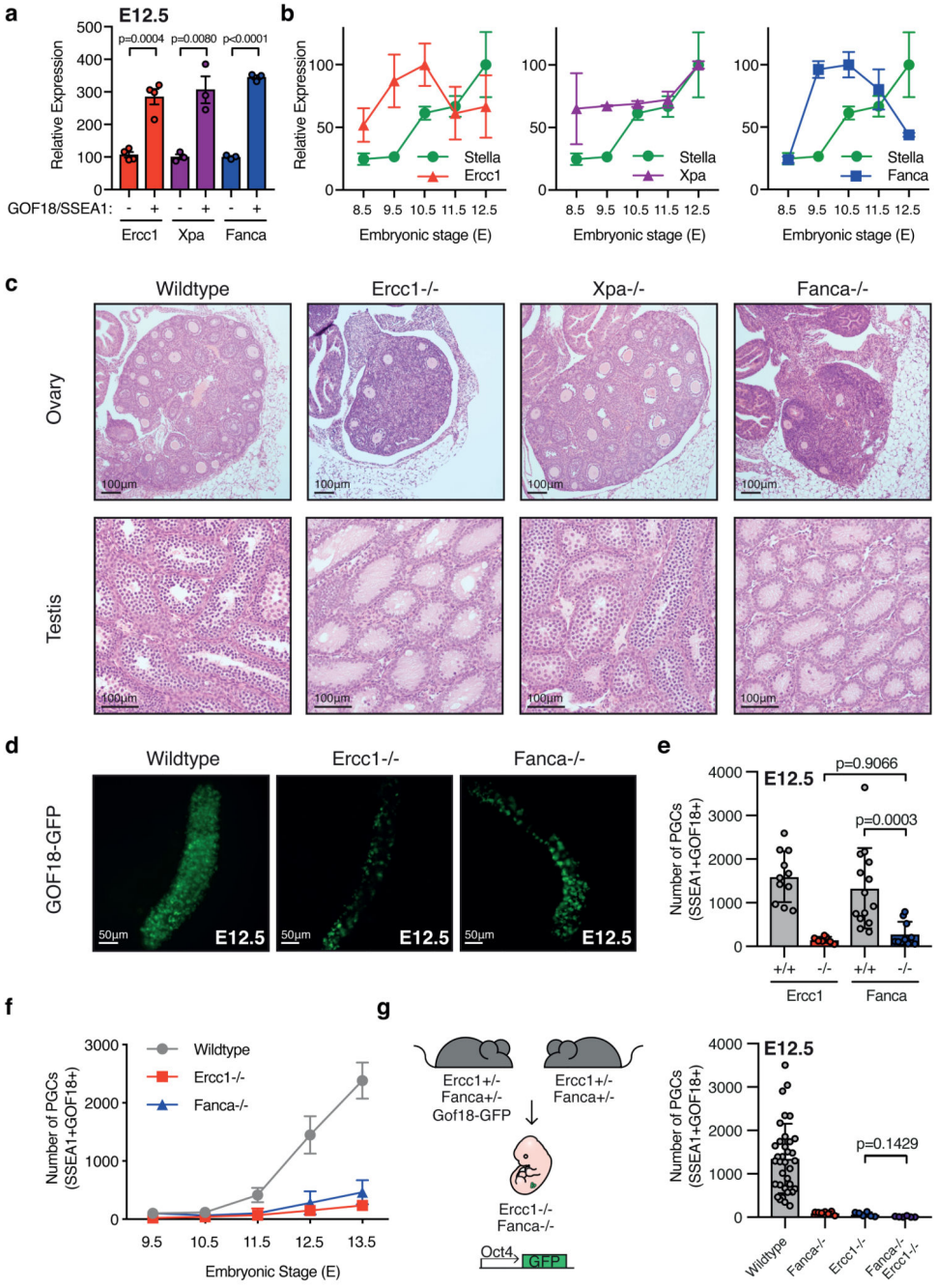

Figure 3. ERCC1 acts together with the Fanconi anemia pathway to preserve PGC development.

a, qRT-PCR expression analysis of the DNA repair genes *Ercc1*, *Xpa* and *Fanca* in surrounding somatic cells (SSEA1$^-$GOF18-GFP$^-$) and PGCs (SSEA1$^+$GOF18-GFP$^+$) purified from E12.5 wildtype embryos (*P* value calculated by 2-tailed Mann-Whitney test; data shown represent mean and s.e.m.; each point represents data from one embryo, $n = 4, 4, 3, ,3 ,3$ and 3, left to right). **b**, qRT-PCR expression analysis of *Ercc1*, *Xpa*, *Fanca* and the germ cell marker *Stella* in PGCs (SSEA1$^+$GOF18-GFP$^+$) during development (E8.5-12.5) (data shown represent mean and s.e.m.; $n = 3$ embryos per genotype per timepoint). **c**, H&E-

Europe PMC Funders Author Manuscripts

stained sections of p14 mice (3 independent animals of each genotype and gender were shown to have similar histology). **d**, Representative images of GOF18-GFP fluorescence in E12.5 gonads (representative data from 3 independent animals per genotype). **e**, Quantification of PGCs ($SSEA1^{+}GOF18\text{-}GFP^{+}$) by flow cytometry from wildtype, *Ercc1*$^{-/-}$ and *Fanca*$^{-/-}$ embryos at E12.5 (*P* value calculated by 2-tailed Mann-Whitney test; data shown represent mean and s.e.m.; each point represents data from one embryo, $n = 11, 7, 14$ and 10, left to right). **f**, Quantification of PGCs ($SSEA1^{+}GOF18\text{-}GFP^{+}$) during embryonic development (E9.5-13.5) by flow cytometry (data shown represent mean and s.e.m.; wildtype $n = 25, 19, 15, 25$ and 25, *Ercc1*$^{-/-}$ n=6, 7, 4, 7, and 14, *Fanca*$^{-/-}$ $n = 7, 6, 13, 10$ and 9 embryos, left to right). **g**, Generation and quantification of PGCs per gonad of *Ercc1*$^{-/-}$ *Fanca*$^{-/-}$ E12.5 embryos (*P* value calculated by 2-tailed Mann-Whitney test; data represent mean and s.e.m.; each point represents data from one embryo, $n = 37, 7, 6$ and 6, left to right).

Europe PMC Funders Author Manuscripts

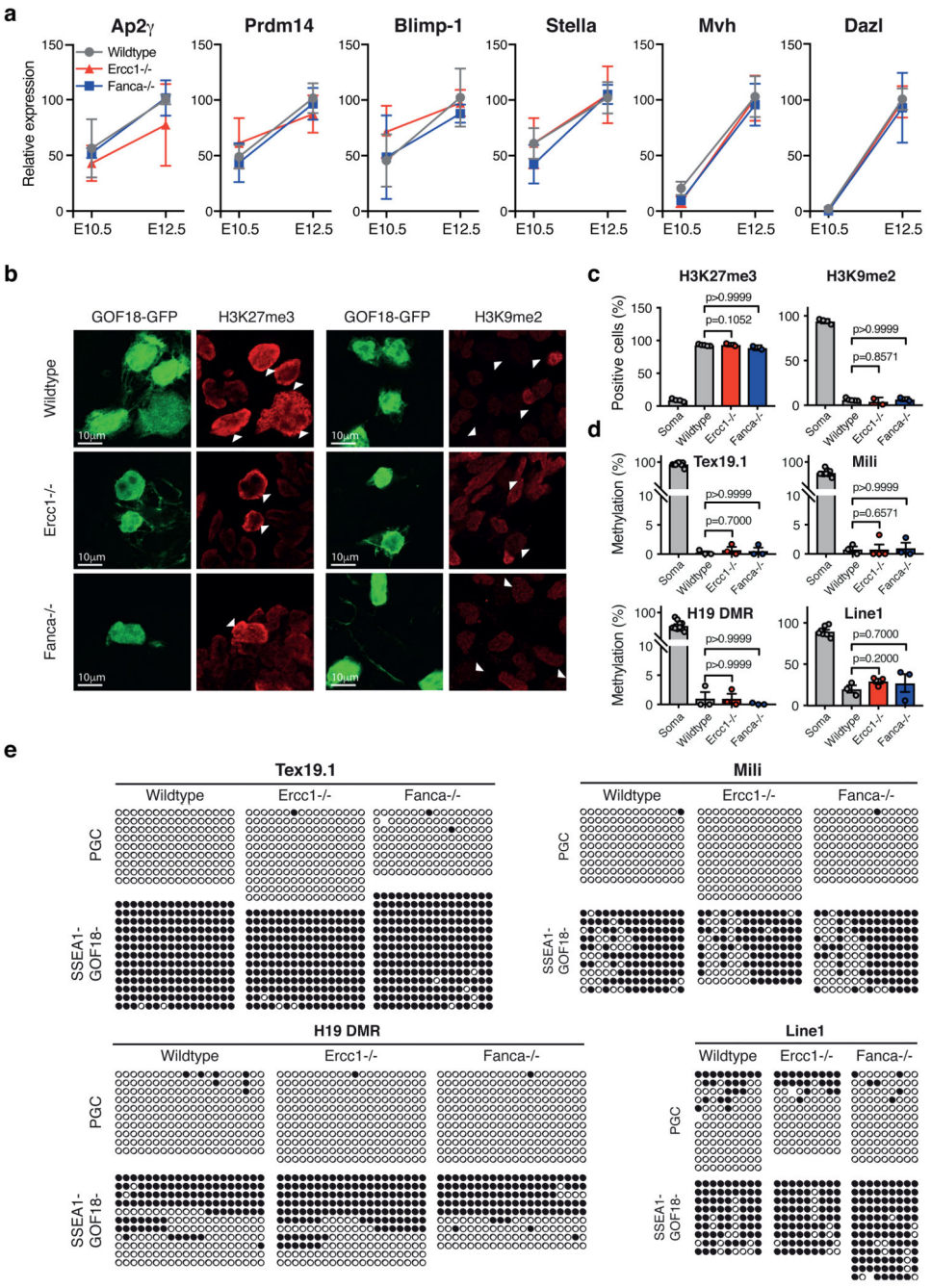

Figure 4. Crosslink-repair-deficient PGCs undergo normal PGC transcriptional activation and epigenetic reprogramming.

a, qRT-PCR expression analysis of early (*Ap2γ*, *Prdm14*, *Blimp-1* and *Stella*) and late (*Mvh* and *Dazl*) germ cell markers in PGCs (SSEA1^{+}GOF18-GFP^{+}) purified from E10.5 and E12.5 wildtype, *Ercc1*$^{-/-}$ and *Fanca*$^{-/-}$ embryos (data represent mean and s.e.m.; $n = 3$ embryos per genotype and timepoint, expression was normalized to *Gapdh* and made relative to the wildtype PGC sample at E12.5 for each gene). Immunofluorescence (**b**) staining and quantification (**c**) of global H3K27me3 and H3K9me2 levels in PGCs (GOF18-

Europe PMC Funders Author Manuscripts

GFP$^+$) and somatic tissue (GOF18-GFP$^-$) in E12.5 genital ridges (*P* value calculated by 2-tailed Mann-Whitney test; data shown represent mean and s.e.m.; each point represents data from one embryo, H3K27me3 *n* = 4, 5, 2, and 2, H3K9me2 *n* = 4, 5, 2, and 2, left to right). **d**, Quantification of DNA methylation of *Tex19.1*, *Mili*,, *H19* and *Line1* transposable elements in fluorescence-activated cell sorted (FACS) PGCs (SSEA1$^+$GOF18-GFP$^+$) and surrounding somatic cells (SSEA1$^-$GOF18-GFP$^-$) (*P* value calculated by 2-tailed Mann-Whitney test; data represent mean and s.e.m.; each point represents data from one embryo, *Tex19.1 n* = 9, 3, 3 and 3, *Mili n* = 9, 3, 4 and 3, *H19 n* = 10, 3, 3 and 3, *Line1 n* = 7, 3, 3, and 3, left to right). **e**, Representative methylation patterns of *Tex19.1*, *Mili*, *H19 DMR* and *Line1* in PGCs (SSEA1$^+$GOF18-GFP$^+$, top) and somatic tissue (SSEA1$^-$GOF18-GFP$^-$, bottom) (closed = methylated CpG, open = unmethylated CpG).

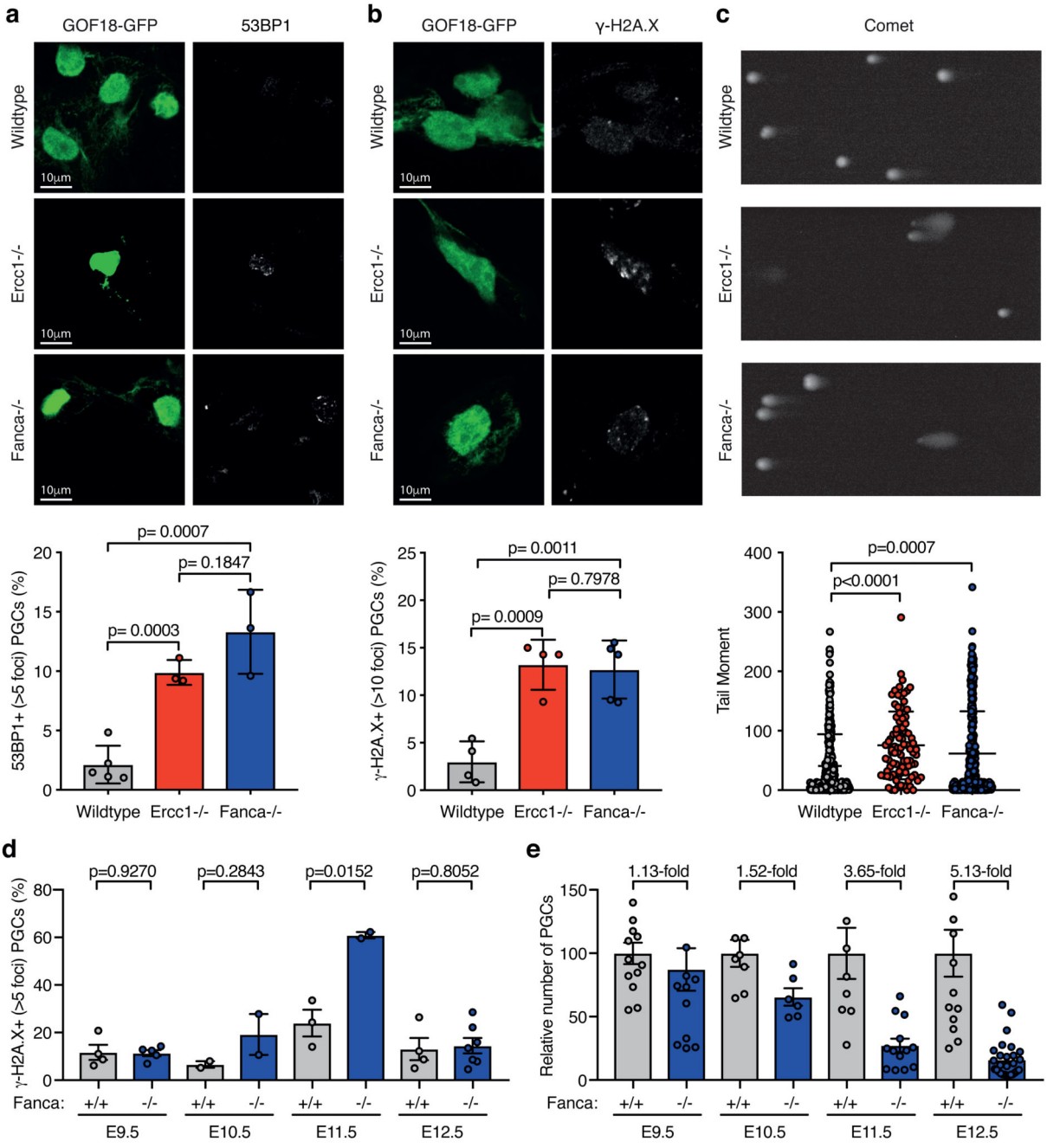

Figure 5. PGCs accumulate unrepaired DNA breaks.

a, Representative images of 53BP1 foci in PGCs (GOF18-GFP$^+$) from embryos at E11.5 and quantification of the frequency of PGCs with > 5 53BP1 foci per nucleus (*P* value calculated by unpaired 2-tailed *t* test; data represent mean and s.e.m.; at least 100 PGCs were scored per embryo, each point represents data from one embryo, $n = 5$, 3 and 3, left to right). **b**, Representative images of γ-H2A.X foci in PGCs (GOF18-GFP$^+$) at E11.5 and quantification of the frequency of PGCs with > 10 γ-H2A.X foci per nucleus (*P* value calculated by unpaired 2-tailed *t* test; data represent mean and s.e.m.; at least 100 PGCs

were scored per embryo, each point represents data from one embryo, $n = 4$, 4 and 5, left to right). **c**, Single-cell electrophoresis of FACS-sorted PGCs (SSEA1^{+}GOF18-GFP^{+}) at E11.5 (*P* value calculated by unpaired 2-tailed *t* test; data represent mean and s.e.m.; at least 100 PGCs were scored per embryo, $n = 3$ embryos per genotype). **d**, Quantification of PGCs (GOF18-GFP^{+}) with > 5 γ-H2A.X foci per nucleus in wildtype or *Fanca*$^{-/-}$ embryos during embryonic development (E9.5-12.5). (*P* value calculated by unpaired 2-tailed *t* test; data represent mean and s.e.m.; each point represents data from one embryo, $n = 4$, 5, 2, 2, 3, 2, 4 and 7, left to right). **e**, Quantification of PGCs (SSEA1^{+}GOF18-GFP^{+}) by flow cytometry in wildtype and *Fanca*$^{-/-}$ embryos during embryonic development (*P* value calculated by 2-tailed Mann-Whitney test; data represent mean and s.e.m.; each point represents data form one embryo, $n = 13$, 13, 8, 6, 9, 13, 14 and 28, left to right).

Europe PMC Funders Author Manuscripts

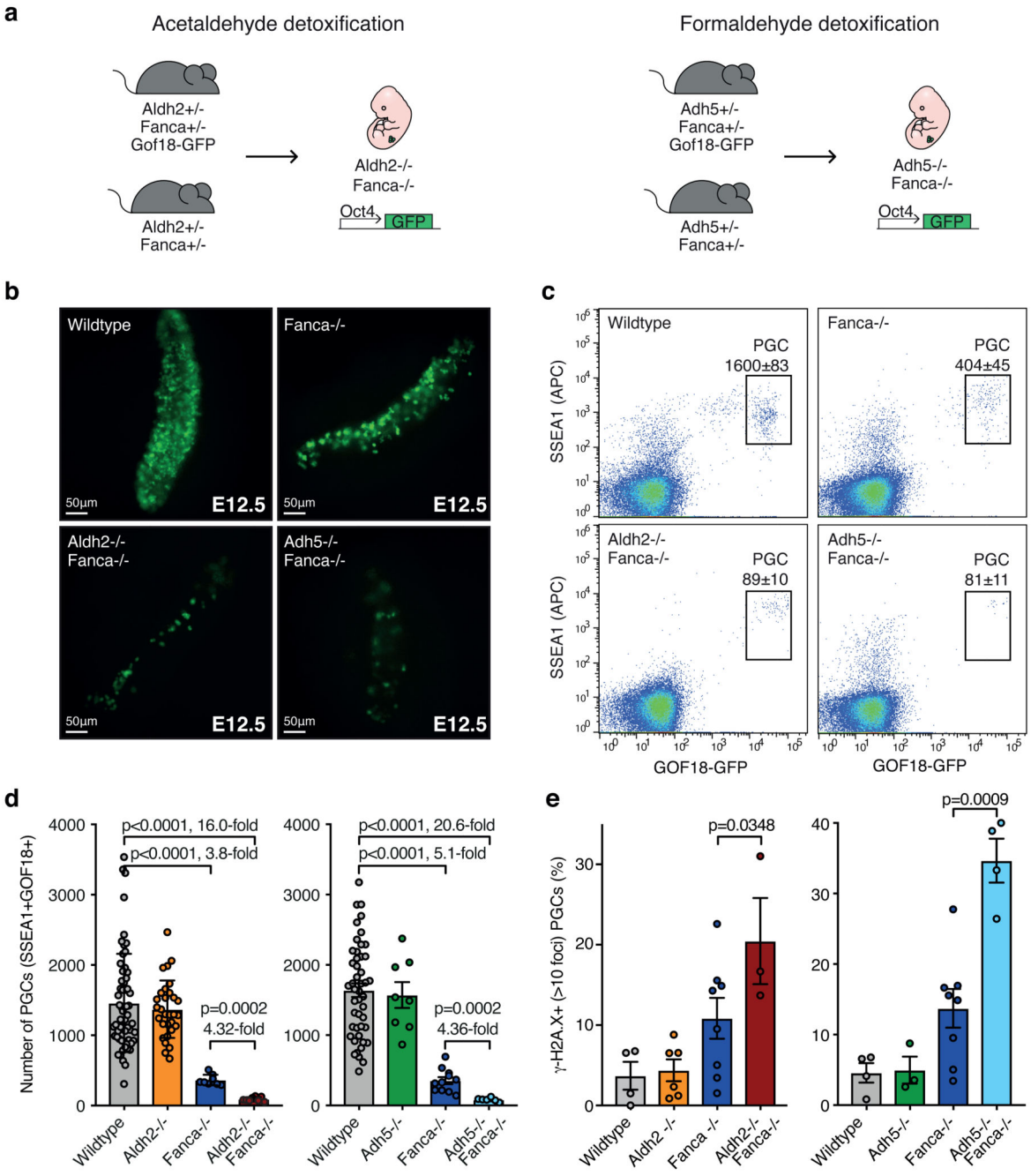

Figure 6. Fetal aldehyde catabolism protects developing PGCs.

a, Generation of embryos that lack both aldehyde detoxification (*Aldh2*$^{-/-}$ or *Adh5*$^{-/-}$) and Fanconi-mediated crosslink repair (*Fanca*$^{-/-}$) carrying the *Gof18-GFP* PGC reporter. **b**, Representative images of GOF18-GFP fluorescence in E12.5 gonads. **c**, Representative flow cytometry plots of PGCs (SSEA1^{+}GOF18-GFP^{+}) from E12.5 embryos. **d**, Quantification of PGCs by flow cytometry from E12.5 embryos (*P* value calculated by 2-tailed Mann-Whitney test; data represent mean and s.e.m.; each point represents data from one embryo *Aldh2*$^{-/-}$ *Fanca*$^{-/-}$ *n* = 60, 30, 8 and 8, *Adh5*$^{-/-}$*Fanca*$^{-/-}$ *n* = 35, 8, 11 and 6, left to right). **e**,

Europe PMC Funders Author Manuscripts

Quantification of PGCs (GOF18-GFP^{+}) with > 10 γ-H2A.X foci per nucleus in E11.5 embryos lacking both acetaldehyde catabolism and ICL repair (*Aldh2*$^{-/-}$*Fanca*$^{-/-}$) or formaldehyde catabolism and ICL repair (*Adh5*$^{-/-}$*Fanca*$^{-/-}$) at E11.5 (*P* value calculated by unpaired 2-tailed *t* test; data represent mean and s.e.m.; each point represents data from one embryo, *Aldh2*$^{-/-}$*Fanca*$^{-/-}$ *n* = 4, 6, 8 and 3, *Adh5*$^{-/-}$*Fanca*$^{-/-}$ *n* = 4, 3, 8 and 4, left to right).

Europe PMC Funders Author Manuscripts

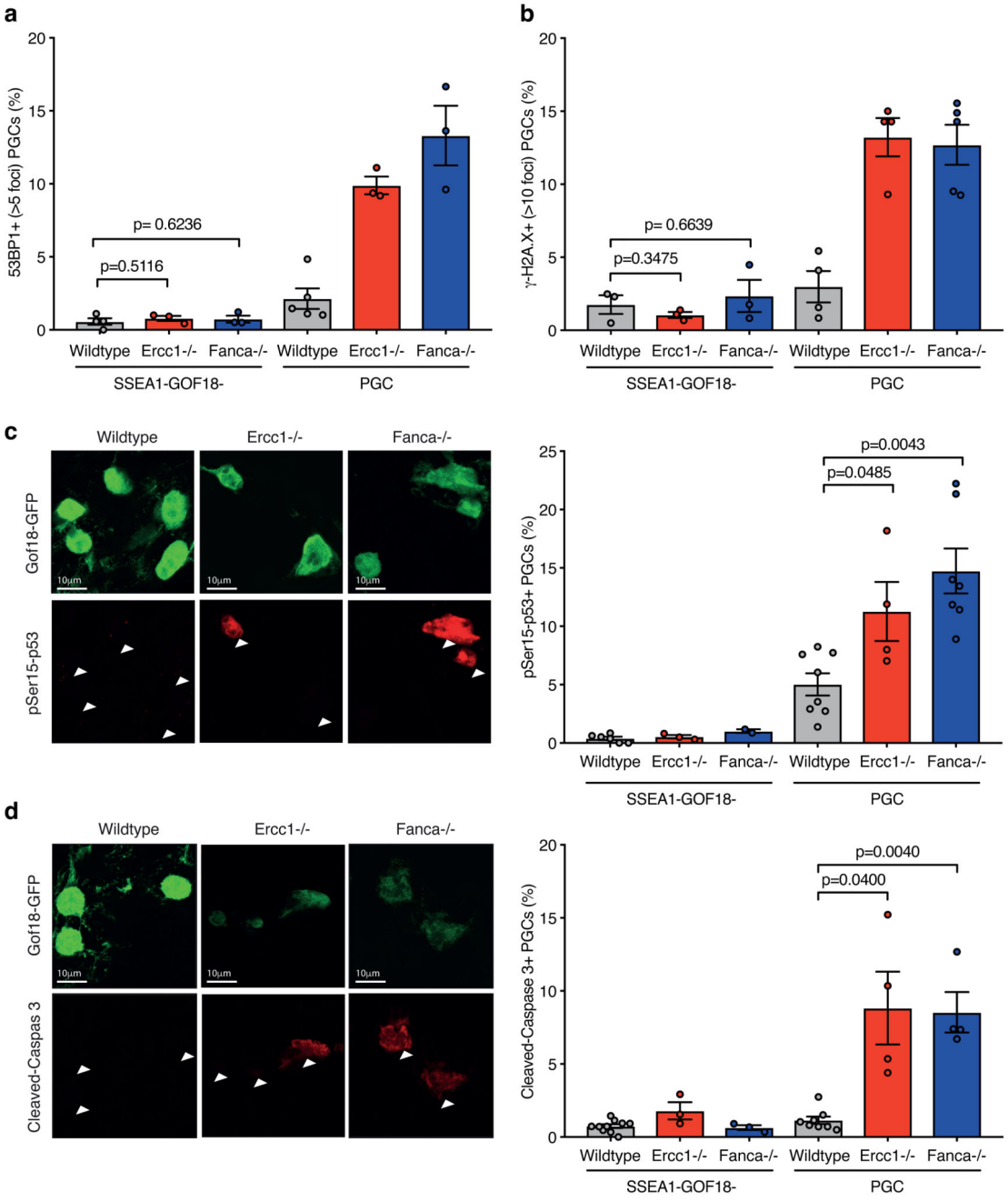

Figure 7. Damaged PGCs are eliminated by apoptosis.

a-b, Quantification of the frequency of PGCs (GOF18-GFP$^+$) and surrounding somatic cells (GOF18-GFP$^-$) with (**a**) > 5 53BP1 or (**b**) > 10 γ–H2A.X foci per nucleus at E11.5. (*P* value calculated by unpaired 2-tailed *t* test; data represent mean and s.e.m.; at least 100 PGCs or somatic cells were scored per embryo, each point represents data from one embryo, 53BP1 *n* = 4, 3, 3, 5, 3 and 3, γ–H2A.X *n* = 3, 3, 3, 4, 4 and 5, left to right). **c**, Representative images of E11.5 gonads stained for phospho-Ser15-p53 (pSer15-p53) and GFP (GOF18-GFP). Quantification of PGCs (GOF18-GFP$^+$) and somatic cells (GOF18-GFP$^-$) that stain

positively for phospho-Ser15-p53 (*P* value calculated by unpaired 2-tailed *t* test; data represent mean and s.e.m.; at least 100 PGCs or somatic cells were scored per embryo, each point represents data from one embryo, $n = 6, 3, 2, 8, 4$ and 7, left to right). **d**, Representative images of E11.5 gonads stained for the marker of apoptosis cleaved-Caspase 3 and GFP (GOF18-GFP) and the quantification of the frequency of PGCs (GOF18-GFP^{+}) and somatic cells (GOF18-GFP^{-}) that stain positively for cleaved-Caspase 3 (*P* value calculated by unpaired 2-tailed *t* test; data represent mean and s.e.m., at least 100 PGCs or somatic cells were scored per embryo, each point represents data from one embryo, $n = 10, 3, 3, 8, 4$ and 4, left to right).

Europe PMC Funders Author Manuscripts